Monthly Notices of the ROYAL ASTRONOMICAL SOCIETY

MNRAS **546,** 1–22 (2026) https://doi.org/10.1093/mnras/stag065
Advance Access publication 2026 January 13

Exploring the quasar disc–wind–jet connection with LoTSS and SDSS

Charlotte L. Jackson [1]★ James H. Matthews [1] Imogen H. Whittam [1,2] Matt J. Jarvis [1,2] Matthew J. Temple [3] Amy L. Rankine [4] and Paul C. Hewett [5]

[1]*Department of Physics, Astrophysics, University of Oxford, Denys Wilkinson Building, Keble Road, Oxford OX1 3RH, UK*
[2]*Department of Physics and Astronomy, University of the Western Cape, Robert Sobukwe Road, 7535 Bellville, Cape Town, South Africa*
[3]*Centre for Extragalactic Astronomy, Department of Physics, Durham University, Durham DH1 3LE, UK*
[4]*Institute for Astronomy, University of Edinburgh, Royal Observatory, Blackford Hill, Edinburgh EH9 3HJ, UK*
[5]*Institute of Astronomy, University of Cambridge, Madingley Road, Cambridge CB3 0HA, UK*

Accepted 2026 January 7. Received 2026 January 7; in original form 2025 October 24

ABSTRACT

We investigate the relationship between disc winds, radio jets, accretion rates, and black hole masses of a sample of ∼100 k quasars at $z \approx 2$. Combining spectra from the 17th data release of the Sloan Digital Sky Survey (SDSS) with radio fluxes from the 2nd data release of the Low Frequency ARray (LOFAR) Two-Meter Sky Survey (LoTSS), we statistically characterize a radio-loud and radio-quiet population using a two-component Gaussian Mixture model, and perform population matching in black hole mass and Eddington fraction. We determine how the fraction of radio-loud sources changes across this parameter space, finding that jets are most efficiently produced in quasars with either a very massive central black hole ($M_{\rm BH} > 10^9\,{\rm M}_\odot$) or one that is rapidly accreting ($\lambda_{\rm Edd} > 0.3$). We also show that there are differences in the blueshift of the C IV λ 1549 Å line and the equivalent width of the He II λ1640 Å line in radio loud and radio-quiet quasars that persist even after accounting for differences in the mass and accretion rate of the central black hole. Generally, we find an anticorrelation between the inferred presence of disc winds and jets, which we suggest is mediated by differences in the quasars' spectral energy distributions. The latter result is shown through the close coupling between tracers of wind kinematics and the ionizing flux – which holds for both radio-loud and radio-quiet sources, despite differences between their emission line properties – and is hinted at by a different Baldwin effect in the two populations.

Key words: accretion, accretion discs – galaxies: active – galaxies: jets – quasars: emission lines – quasars: general – radio continuum: galaxies.

1 INTRODUCTION

Quasars are some of the most extreme objects in the Universe, with luminosities reaching up to $\sim 10^{41}$ W ($\sim 10^{48}$ erg s^{-1}; P. Padovani et al. 2017), and central supermassive black holes with masses of up to 10^{10} M$_\odot$ (X.-B. Wu et al. 2015). Originally, quasars were discovered as anomalous sources with enormous luminosities across many frequencies, particularly in the radio, but with only a point-like optical counterpart, morphologically similar to a distant star (M. Schmidt 1969; K. I. Kellermann et al. 1989). However, despite radio emission playing a critical role in their original identification, we know now that many quasars are very faint or undetected in the radio (A. Sandage 1965; M. J. Kukula et al. 1998), and amongst those that do show strong emission, many host impressive extended structure in the form of (ultra)relativistic collimated polar radio jets. Exactly the mechanism or physical characteristic of a quasar that determines whether it will launch a jet is yet to be precisely established. Furthermore, whilst it is also thought that quasars often form another type of energetic outflow, wide-angled winds, how these co-exist or interact with formation of jets is not fully understood. The third crucial part of the puzzle is how these two types of outflow connect to the underlying accretion physics of the quasar.

1.1 Quasar outflow physics

There are two dominant theoretical models for the launching of quasar jets: one that is black hole driven (R. D. Blandford & R. L. Znajek 1977, BZ), and another that derives energy from the accretion disc instead (R. D. Blandford & D. G. Payne 1982, BP). The BZ mechanism involves the extraction of rotational energy from the central supermassive black hole via a strong poloidal magnetic field with open field lines threading the event horizon (R. Y. Talbot, M. A. Bourne & D. Sijacki 2021). On the other hand, in the BP process, the energy fuelling a radio jet is instead

★ E-mail: charlotte.jackson@physics.ox.ac.uk

extracted from the accretion disc by magnetic fields threading the disc, and the jet is launched centrifugally (W. Xie et al. 2012). Key differences between these two launching mechanisms include the region of influence of the magnetic field (in the BP process, the field must be distributed across a large radial extent of the disc, whereas in BZ, it is only important at the black hole's ergosphere; J. Ferreira, P.-O. Petrucci & Q. Garnier 2013); the spin dependence of the launching (the BZ mechanism strictly requires the black hole to be spinning, which is not the case for BP); and the efficiency of jet formation (it is thought that a BZ-like process would result in a significantly higher efficiency than a BP-like one; R. S. Nemmen & A. Tchekhovskoy 2015).

The BP mechanism can also be invoked as an explanation for the launching of accretion disc winds in quasars. In that picture, gas is ejected by centrifugal forces along the field lines threading the disc (M. Wardle & A. Koenigl 1993; A. Konigl & J. F. Kartje 1994). This is the magnetohydrodynamic (MHD) wind launching mechanism, and whilst there is good reason to expect that it may play an important role in outflows from the accretion disc, it is unclear currently what the observational signatures of the wind might look like, due to their dependence on the illusive magnetic field configuration in the disc (e.g. R. D. Blandford & D. G. Payne 1982; J. E. Everett & D. R. Ballantyne 2004; K. Fukumura et al. 2018).

Winds can also be launched via thermal pressure (S. Laha et al. 2021). Thermally driven winds occur when X-rays produced in the inner accretion disc irradiate the outer disc, bringing material up to the Compton temperature, at which point it expands and becomes a thermally driven wind at radii where the local escape velocity is exceeded by the sound speed in the material (M. C. Begelman, C. F. McKee & G. A. Shields 1983; D. T. Woods et al. 1996; M. Mizumoto et al. 2019).

The third commonly considered launching mechanism is radiative line driving. The governing principle is that bound electrons in a plasma provide a greater-than-Thomson cross-section to incident light (L. B. Lucy & P. M. Solomon 1970; J. I. Castor, D. C. Abbott & R. I. Klein 1975; S. P. Owocki, S. R. Cranmer & J. M. Blondin 1994). Crucially, for substantial momentum transfer to occur, there must be a delicate balance in the quasar spectral energy distribution (SED). A strong driving (near-) ultraviolet flux is needed to produce the required radiation pressure, alongside limited extreme-ultraviolet (EUV) and X-ray production to prevent overionizing the gas (N. Murray et al. 1995; N. Higginbottom et al. 2014; M. J. Temple et al. 2023).

1.2 Observational signatures of outflows

The tendency for quasars to emit prodigiously across the entire electromagnetic spectrum allows for rich analyses probing their physical processes (M. Elvis et al. 1994). In the standard picture of a quasar (i.e. that of D. E. Osterbrock 1993; B. M. Peterson 1997; V. Beckmann & C. R. Shrader 2012; P. Padovani et al. 2017, etc.), emission of different wavelengths comes from different physical regions. In particular, ultraviolet and optical emission is thought to be produced primarily in the accretion disc, whereas X-rays are emitted from the innermost region of the disc, the so-called X-ray corona, and infrared emission is produced by the absorption and subsequent remission from a dusty torus. Observations at radio wavelengths can uncover sources of synchrotron emission, such as in jets, winds or shocks, and are not subject to absorption by dust due to their long wavelengths.

Spectroscopy can provide great insight into a quasar's inner working through the observable properties of important emission and absorption lines. Outflows in the form of disc winds can be inferred by the presence of broad absorption lines or the blueshift of the C IV λ1549 Å emission line (D. Proga, J. M. Stone & T. R. Kallman 2000; K. M. Leighly & J. R. Moore 2004; G. T. Richards et al. 2011). C IV is a collisionally excited line formed in the broad-line region (BLR) of a quasar, which is commonly observed to be blueshifted with respect to its expected laboratory wavelength. Whilst the exact cause of this blueshift is still under investigation (e.g. J. H. Matthews et al. 2023), a common assumption is that this is a signature of outflowing material, often interpreted as a disc wind.

There is also a strong inverse correlation between the equivalent widths (EWs) of various ultraviolet emission lines, including C IV, and the ultraviolet continuum luminosity, known as the 'Baldwin effect' (J. A. Baldwin 1977). G. T. Richards et al. (2011) showed that $EW_{C\ IV}$ also anticorrelates with the strength of the blueshift of the C IV line. Unfortunately, the part of the SED responsible for ionizing such lines, the EUV, is generally inaccessible due to absorption along the line of sight (J. D. Timlin, W. N. Brandt & A. Laor 2021). Fortunately, the He II λ1640 Å line is a simple, single-electron process, produced by the recombination of He III to He II. It provides a relatively 'clean' measure of the number of incident photons with an energy high enough to create He III, which is 54.4eV and above, as the ratio of photons produced by recombination and subsequent line emission is of the order of unity. Therefore, the relative strength of the He II line, measured by its EW, is a good 'photon counter' for the ionizing EUV flux (W. G. Mathews & G. J. Ferland 1987; A. Baskin, A. Laor & F. Hamann 2013; A. L. Rankine et al. 2020; M. J. Temple et al. 2023).

Radio emission in quasars is associated with a wide range of processes, and displays the most dynamic range in luminosity of all electromagnetic wavelengths, spanning from essentially non-existent to 10^{30} W Hz^{-1}. For the very highest radio luminosities, it is clear that the dominant source of radiation has its origins in jets carrying relativistic electrons (A. Laor & E. Behar 2008), but for those sources at low and more intermediate radio luminosities, the primary source of the emission is less clear (see F. Panessa et al. 2019, for a review). Previous studies have suggested that it could come from the X-ray corona (A. Laor & E. Behar 2008), relativistic particles accelerated in shocks within outflows (N. L. Zakamska & J. E. Greene 2014; J. Nims, E. Quataert & C.-A. Faucher-Giguère 2015), star formation (J. J. Condon 1992; M. Bonzini et al. 2015; P. Padovani 2016; D. J. Rosario et al. 2020), or weak/ frustrated jets (G. V. Bicknell 2002; J. W. Broderick & R. P. Fender 2011). These processes will presumably also play a role luminous radio quasars, just a sub-dominant one. Historically, sources have been divided into two populations: those that have very strong radio emission originating in a high-power jet, and those that have not. These are often referred to as 'radio loud' (RL) and 'radio quiet' (RQ), respectively. The existence of a true dichotomy in the distribution of radio properties of quasars has been the focus of intensive study for many years (e.g. J. J. Condon et al. 1980; R. Moderski, M. Sikora & J. P. Lasota 1998; R. McLure & J. Dunlop 2001; M. Cirasuolo et al. 2003; P. P. B. Beaklini et al. 2020; L. Zhang, J. Fan & J. Zhu 2021; C. Macfarlane et al. 2021), as has the question of what determines whether a quasar will be RL or RQ. So far, there have been no properties, outside of their radio emission, that have been identified as an

accurate predictive tool of the radio loudness of an individual quasar.

1.3 Motivation and aims of this study

There remain several key questions still to be answered in order to fully understand the outflow properties of quasars. Why do some quasars launch jets, but not others? How are quasar jets and disc winds launched, and what is the connection between these two modes of outflow? How do the outflow properties of a quasar relate to its accretion physics? Many authors have sought to better understand the answers to these questions; particularly relevant to our work are several recent studies focusing on emission line 'demographics', building on the work of G. T. Richards et al. (2011). A. L. Rankine et al. (2021) studied the connection between radio and outflow properties of quasars, finding differences in the C IV and He II emission lines of RL and RQ objects, yet also sources with similar ultraviolet properties but strikingly different radio emission. M. J. Temple et al. (2023) also found population-level differences in emission line properties, but this time focusing on the connection with accretion rate and black hole mass. In particular, they find a regime at high black hole mass and accretion rate that is associated with the strongest disc winds and softest SED, along with a prominent switch in ultraviolet emission line behaviour at an Eddington fraction of $\simeq 0.1$. J. W. Petley et al. (2024) suggest that different outflow processes dominate in quasars as a function of C IV blueshift and $\mathrm{EW_{C\ IV}}$, which they argue offers a proxy to Eddington-scaled accretion rate. They point to high accretion rates corresponding primarily to disc wind-caused radio emission, and lower accretion rates associated with emission dominated by radio jets. These three specific works fit within a broader landscape of literature exploring how the radio emission in quasars depends on, for example, C IV emission line properties (G. T. Richards et al. 2011, 2021; R. M. Kratzer & G. T. Richards 2015; G. Calistro Rivera et al. 2024), colour/dust extinction (R. L. White et al. 2003; L. Klindt et al. 2019; V. A. Fawcett et al. 2020; D. J. Rosario et al. 2020; V. A. Fawcett et al. 2023) and the presence or absence of broad absorption lines (J. T. Stocke et al. 1992; P. C. Hewett & C. B. Foltz 2003; L. K. Morabito et al. 2019; J. W. Petley et al. 2022).

In our work, we connect these previous studies and further investigate the relationship between radio emission, accretion disc outflows, and fundamental properties of quasars, including Eddington fraction and black hole mass. The aim of this paper is to compare observational signatures of disc winds, radio jets, and the accretion disc in quasars. We use a combination of rest-frame ultraviolet spectroscopy with deep low frequency radio observations across ∼100 000 optically identified quasars, with a redshift range of $1.5 < z < 2.65$, that gives coverage of the C IV, He II, and Mg II emission lines within the Sloan Digital Sky Survey (SDSS) observational window. In Section 2, we present the observational data and detail how our radio-loud sample is defined. Our key results are presented in Section 3, and we discuss their physical consequences in Section 4. Throughout the paper, we give wavelengths in vacuum in units of Ångstrom, black hole masses in $\mathrm{M_\odot}$, and luminosities in $\mathrm{W\,Hz^{-1}}$. We assume a flat Lambda cold dark matter (ΛCDM) cosmology with $H_0 = 71\,\mathrm{km\,s^{-1}Mpc^{-1}}$. Energies, frequencies and wavelengths are given in the rest frame.

2 OBSERVATIONAL DATA AND METHOD

2.1 Observational data

We use the sub-sample of quasars from the SDSS DR17, described by B. W. Lyke et al. (2020) and Abdurro'uf et al. (2022), that was constructed by M. J. Temple et al. (2023). In their work, they carried out spectral reconstructions, based on the Mean-Field Independent Component Analysis performed by A. L. Rankine et al. (2020), and extracted spectroscopic redshifts and the emission line properties of C IV, He II, and Mg II. 186 303 sources were both in the redshift range of $1.5 < z < 2.65$ and met their spectral quality criteria. See M. J. Temple et al. (2023) and A. L. Rankine et al. (2020) for full details on the sample processing.

Radio data for our sample are taken from the LOFAR Two-meter Sky Survey (LoTSS) DR2, described by T. W. Shimwell et al. (2022). LoTSS is a wide-area radio survey operating at 144 MHz, with a sensitivity of 71 $\mu\mathrm{Jy\ beam^{-1}}$. The second data release provides a catalogue of nearly 4.5 million sources at 6 arcsec resolution, covering 27 per cent of the Northern sky, observing nearly an order of magnitude more sources than DR1. There is also excellent multiwavelength coverage across the observing area of LoTSS, including significant overlap with SDSS DR17.

To obtain a combined radio and rest-frame ultraviolet catalogue, we cross-match the SDSS sample from M. J. Temple et al. (2023) with the value-added LoTSS DR2 source catalogue described by M. J. Hardcastle et al. (2023), using the positions of the established optical counterparts of the radio sources. We first identified the sub-set of the quasar catalogue lying within the sky coverage of LoTSS DR2, an exercise which reduces the sample from 186 303 sources to 108 167. The sky coverage of the two data sets and the subsequently trimmed SDSS catalogue can be seen in Fig. 1. We then cross-matched the two catalogues with a 1 arcsec error radius. The cross-matching resulted in 15 255 radio detected quasars, with a radio detection fraction of 15 per cent, which is similar to the results of A. L. Rankine et al. (2021), who cross-matched the LoTSS DR1 sample (T. W. Shimwell et al. 2019) with SDSS DR14, and found an overall detection fraction of 16 per cent. The luminosities of the quasars in our sample spans a range of $L_{144} \approx 10^{24-29}\,\mathrm{W\,Hz^{-1}}$.

For the other 92 912 objects below the 5σ LoTSS peak detection limit, we extract a radio flux density using forced photometry. In previous studies, the survey detection limit has been used to produce an upper bound on the radio luminosity of undetected sources, allowing them to be used in the radio quiet population, for example in A. L. Rankine et al. (2021). In this work, we elect to retrieve a flux density measurement directly from the LoTSS image to gain insight into the radio emission occurring below the catalogue threshold, and to confirm that these quasars are definitely radio quiet by all definitions. We downloaded 30 arcsec radio cut-outs from the LOFAR API service,[1] centred on their SDSS coordinates. The flux at the central pixel is extracted, and the median flux of 500 randomly selected pixels in the cutout is calculated as the background noise. The difference between the two is then taken as their radio flux density, which allows us to add the radio measurements of an additional 70 292 sources to our sample. The central flux density of our undetected sources is taken as a good approximation for total flux as it is assumed that,

[1]Information available at https://LOFAR-surveys.org/cutout_api_details.html.

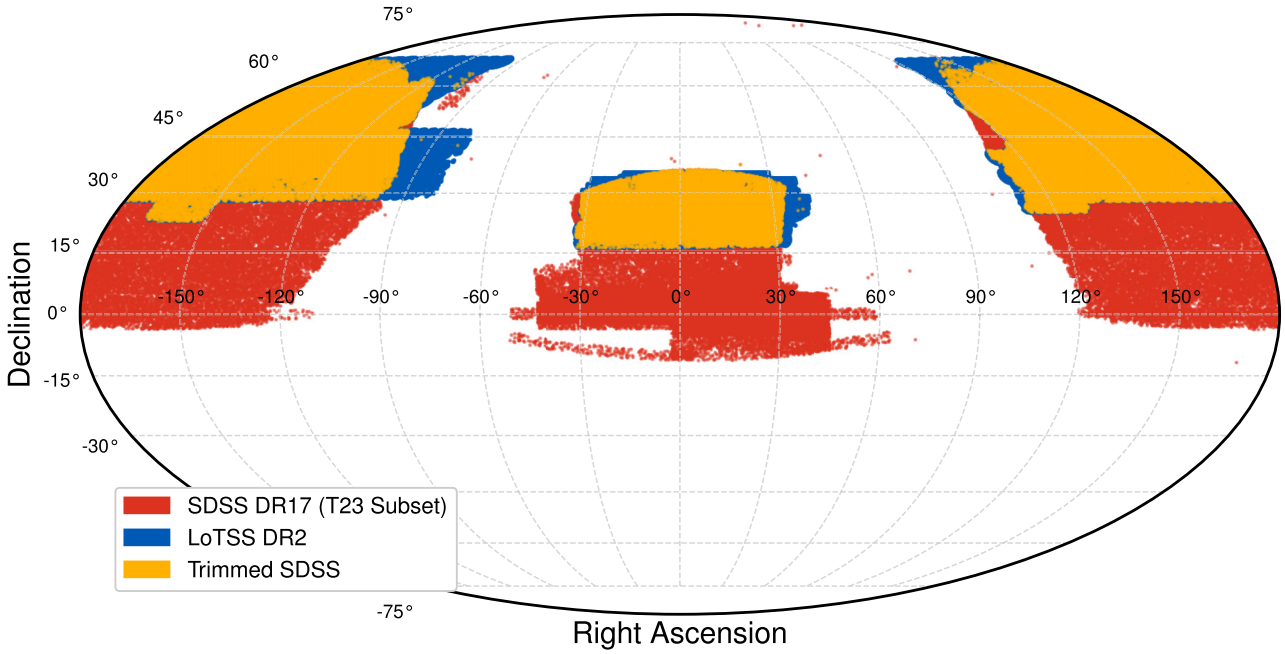

Figure 1. Sky coverage of the surveys used in this work. The Sloan Digital Sky Survey DR17 sub-set constructed by M. J. Temple et al. (2023) (red), LOFAR Two-Meter Sky Survey DR2 optical identifications catalogue (blue), and the resulting overlapping sample (yellow).

if undetected in the LoTSS DR2 catalogue, the quasars are very likely to be unresolved point sources in the radio image, and as the radio image pixels are calibrated in flux/beam, it is ensured that, for unresolved sources, the peak flux is necessarily equal to the total flux. We verified that the pixel fluxes provide a good estimate of the total flux for the faintest sources in the detected sample.

The black hole masses of the quasars in our sample are taken from the M. J. Temple et al. (2023) catalogue, which used the single epoch virial estimator described by R. J. McLure & M. J. Jarvis (2002) and later M. Vestergaard & P. S. Osmer (2009), as seen in equation (1),

$$M_{\rm BH} = 10^{6.86} \left(\frac{\rm FWHM_{Mg\ II}}{1000\,\rm km\,s^{-1}} \right)^2 \left(\frac{L_{3000}}{10^{44}\rm erg\,s^{-1}} \right)^{0.5} \rm M_\odot\,, \quad (1)$$

where $\rm FWHM_{Mg\ II}$ is the full-width at half maximum of the Mg II line, and L_{3000} is the rest-frame monochromatic continuum luminosity at 3000 Å. Mg II is a strong, broad, low-ionization line; the FWHM of which is thought to trace the viralized bulk motion of the emitting BLR. It is also known from reverberation mapping measurements (e.g. A. Wandel, B. M. Peterson & M. A. Malkan 1999; S. Kaspi et al. 2000) that there is a generally constant relationship between the physical size of the BLR and the observed UV luminosity, which R. J. McLure & M. J. Jarvis 2002 demonstrated is particularly tight for L_{3000}. As such, the combination of these two properties can offer an estimation of the black hole mass of a quasar, through virial arguments. To ensure self-consistency, we therefore use L_{3000} throughout the paper, including in the calculation of bolometric luminosity, $L_{\rm bol} = 5.15 \times L_{3000}$, assuming a constant bolometric correction (G. T. Richards et al. 2006; Y. Shen et al. 2011). L_{3000} has the advantage over monochromatic line luminosities (e.g. [O III], H β) of offering a more direct view of a quasar's thermal luminosity (i.e. the 'big blue bump'; B. Punsly & S. Zhang 2011). However, there are still multiple assumptions embedded in the use of constant bolometric correction, an overall discussion of which is given in section 5.1.1 of M. J. Temple et al. (2023). The Eddington fraction is then calculated as the ratio of a source's bolometric luminosity to its Eddington luminosity, $L_{\rm bol}/L_{\rm Edd}$, herein $\lambda_{\rm Edd}$, given by

$$\lambda_{\rm Edd} = \frac{L_{\rm bol}}{L_{\rm Edd}} = \frac{5.15 \times L_{3000}}{1.26 \times 10^{38} \left(\frac{M_{\rm BH}}{\rm M_\odot} \right) \rm erg\,s^{-1}}\,. \quad (2)$$

The monochromatic radio luminosity at 144 MHz are calculated as

$$L_{144} = 4\pi d_L^2 S_{144\rm MHz} (1+z)^{-\alpha-1} \rm W\ Hz^{-1}\,, \quad (3)$$

where d_L is the luminosity distance, $S_{144\rm MHz}$ is the flux at 144 MHz, z is the redshift, and α is the spectral index. Throughout the paper, we use $F_\nu \propto \nu^\alpha$, where α is assumed to be -0.7 (M. J. Kukula et al. 1998).

2.2 Defining a 'jetted' population

In the absence of high resolution very long baseline interferometry imaging and subsequent morphological classification for each of the ∼100 K objects, the identification of radio jets becomes a task of inference rather than direct observation.

Standard practice for some time has been to divide quasars into two populations based on the 'radio loudness' of a source, as defined by the ratio $R = \frac{L_{\rm rad}}{L_{\rm opt}}$, which normalizes the radio luminosity by the optical luminosity. The normalization allows for the identification of sources dominated by radio emission, rather than being biased towards those that are simply intrinsically brighter at all wavelengths. However, there are associated pitfalls with the method. First, there is the decision of where to place a cut-off between 'radio loud' and 'radio quiet' populations in a distribution which, with the development of deeper and more sensitive radio surveys such as LoTSS, has become increasingly continuous – see. Fig. 2. Too low a division, and non-jetted sources with strong radio emission originating from other processes, such as

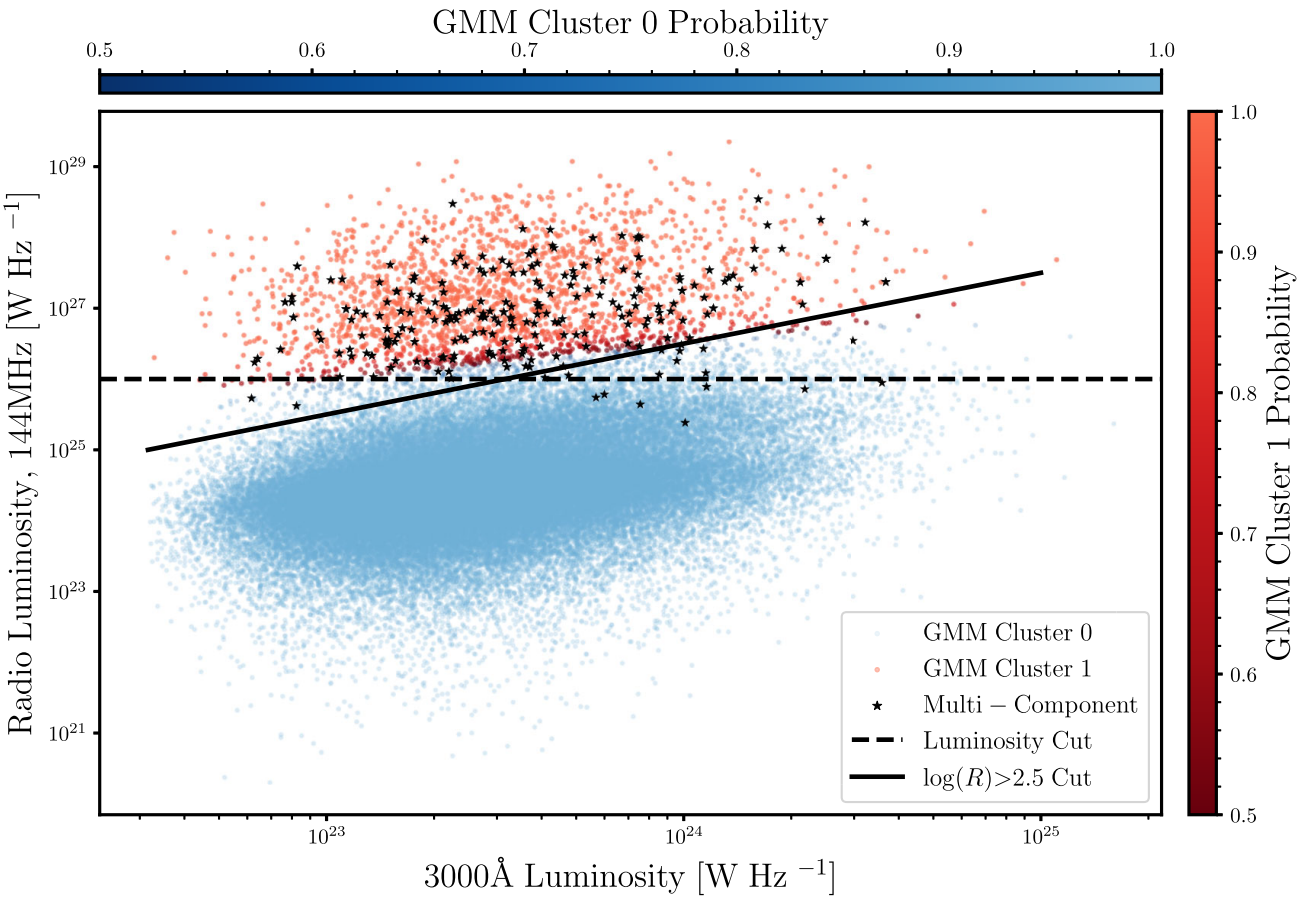

Figure 2. Distribution of quasars in L_{3000} and 144 MHz radio luminosity. The colour of the points corresponds to the cluster to which the source has been assigned by the two-component GMM, with Cluster 1 (red) defining radio-loud and Cluster 2 (blue) defining radio-quiet sources. The shading of the points indicates the probability of the source being correctly assigned to its cluster, with darker colours showing less certainty. The solid black line shows the classical radio loudness cut at $\log_{10}(R) > 2.5$, and the dashed line indicates the 10^{26} W Hz^{-1} radio luminosity cut. The stars show sources with multiple (>1) associated components in the LoTSS DR2 value-added catalogue.

star formation, will contaminate the sample. Too high, and it risks missing weaker jets, particularly where there is relatively strong optical emission. Secondly, there is the interdependency between the ratio and other values that are calculated from the optical luminosity, such as black hole mass and Eddington fraction. As a result, it is more difficult for a source to meet the threshold if it has a higher black hole mass, based on its higher optical luminosity at fixed Eddington fraction, see equation (1).

One option to lift the optical luminosity dependency is to use a purely radio luminosity-based cut, which is more reminiscent of early work (e.g. L. Miller, J. A. Peacock & A. R. G. Mead 1990; P. N. Best 2007). Whilst the approach may result in an overrepresentation of sources that are simply the most intrinsically bright across all wavelengths, it should equally feature some of the more intermediate luminosity jets. However, this method is not used often in modern studies as it does not account for any correlations between radio and optical luminosities (e.g. M. Baloković et al. 2012), and relies on a relatively arbitrary placement for the cut.

Ideally, one would define a method to classify a jetted population based on the distribution of sources in the optical and radio luminosity plane, looking for a general minimum across the 2D distribution, which may not be linear. Previous works have sought to address this challenge, including B. H. Yue et al. (2024, 2025), who used a parametric model describing the active galactic nucleus (AGN) and star formation contributions to a population's radio emission in an effort to statistically disentangle them. Another option, and the one we choose to use in this study, is to use a Gaussian Mixture Model (GMM), that fits Gaussian components to the overall distribution of sources, and defines 'clusters'. As such, the statistical significance of the populations can be ascertained, and probabilities for each source being in each population quantified – moving away from a blunt classifier based on a chosen cut location.

For the purposes of this study, we choose to define a 'radio loud' and 'radio quiet' population using each of these three methods, and present the results of these classifications in Fig. 2. We choose to use a GMM with two components, which is motivated by the distribution of the data and which has the benefit of producing RL and RQ analogues that are directly comparable to the use of a radio loudness or luminosity cut. However, many more Gaussians could in theory be fitted to the distribution, for example defining a 'radio intermediate' cluster. Throughout this paper, we will discuss the impact of these different definitions.

We calculate the classical radio loudness parameter, R, of each source using the radio luminosity derived from a combination of the catalogue and measured radio flux densities, along with the spectroscopic redshifts of the quasars. We use the rest-frame monochromatic continuum luminosity at 3000 Å for $L_{\rm opt}$, derived

Table 1. The number of sources classified as radio loud and radio quiet for each of the three characterization methods. The identification column shows how many sources with multiple associated components in the radio catalogue have been classified as radio loud per method, which we use as a test for success. Particularly, the GMM identifies the same number of multicomponent objects for the fewest overall RL classifications, suggesting that it may be the most efficient.

Cut used	RL	RQ	Identified
$\log_{10}(R) > 2.5$	2383	105 784	221/231
$L_{144} > 10^{26}$W Hz^{-1}	2577	105 590	227/231
GMM	2014	106 153	221/231

from M. J. Temple, P. C. Hewett & M. Banerji (2021)'s quasar SED model. The choice of radio loudness cut-off location depends largely on the scientific question aiming to be answered. In this work, we seek to isolate a population of jetted quasars, so choose a relatively strict cut of $\log_{10}(R) = 2.5$, which corresponds to a minimum in the distribution of the L_{144} and L_{3000} (see Fig. 2). It also depends heavily on the radio frequency used for observations, and therefore a spectral index assumption. The canonical threshold is $\log_{10}(R) = 1$ at 5 GHz (K. I. Kellermann et al. 1989), and at LOFAR frequencies, often a value of $\log_{10}(R) > 2$ is used. However, it should be noted that A. L. Rankine et al. (2021) uses the SDSS *i*-band magnitude, which is not the same as our L_{3000} measurement. Our choice of cut undoubtedly means that jetted sources 'leak' into the RQ population, but it is reasonable to assume that the RL subsample is relatively clean. With the cut applied, out of the 105 784 sources in our sample, 2383 are classified as RL (a global proportion of 2.20 per cent), and the other 105 784 as RQ (see Table 1).

We also define RL and RQ populations based on the radio luminosity of our sources, removing any dependence on the emission from the accretion disc. We use $L_{144} > 10^{26}$W Hz^{-1}, above which, the radio emission is unlikely being produced by star formation alone. According to the relationship found by G. Calistro Rivera et al. (2017),

$$L_{\mathrm{SFR,144MHz}} = \mathrm{SFR}[\mathrm{M}_\odot/\mathrm{yr}] \times 1.455 \times 10^{24} \times 10^{-q(z)}\mathrm{W\ Hz}^{-1}, \quad (4)$$

where $q(z) = 1.77(1+z)^{-0.22}$, a radio luminosity of $L_{144} > 10^{26}$W Hz^{-1} would correspond to a rate on the order of 3000 $\mathrm{M}_\odot\mathrm{yr}^{-1}$, which is an order of magnitude greater than found in studies such as D. J. E. Floyd et al. (2013) and K. Harris et al. (2016). The criteria yields a global proportion of 2.38 per cent RL sources, the highest of the three methods. The trend of increasing L_{144} with L_{3000} means that sources are more likely to meet the threshold if they have a greater bolometric luminosity.

Finally, we employ a GMM from SCIKIT LEARN (F. Pedregosa et al. 2011) with two components and a tied covariance matrix, for the sources in our sample with positive radio flux densities. Those with negative fluxes are automatically assigned to the RQ population, and are naturally included in the RQ classification of the other methods. Encouragingly, the two Gaussian components that fit to the $L_{\mathrm{rad}} - L_{3000}$ distribution define clusters that are similar to the traditional radio loudness classifications. Almost all objects that are defined by the GMM as being RL meet the $L_{144} > 10^{26}$W Hz^{-1} criteria, and 1.86 per cent of all sources are classified as RL. Furthermore, we are also able to assign a probability of each source being in the associated clusters. We use these as weights instead of a binary classification in the following analyses, as detailed in the results.

In the absence of an accessible 'ground truth' about which sources have jet activity, we use the LoTSS DR2 component catalogue produced by M. J. Hardcastle et al. (2023) to identify sources with multiple associated components, which is an indicator of extended structure, and test whether the three classification methods 'recover' these sources. However, extended structure is not guaranteed to be *jetted* structure, and there are most certainly sources with jets missing from the classification. Therefore, we both can neither take a classification of 'multicomponent' as the smoking gun of a jet, nor the lack of classification as confirmation there is no jet present; nevertheless, the exercise acts as a reasonable sanity check. We find 231 objects present in our sample that have multiple components, which are overplotted on Fig. 2. We present in Table 1 the recovery rate for each classification method, which is consistent across all three and shows that, in general, each method is successful at finding jetted sources. There are four sources with multiple components that are not recovered at all, but these do not show convincing signs of jet activity in their radio image cutouts. The GMM classifies the least number of quasars as RL, but still recovers the same number of multicomponent sources at the traditional radio loudness cut, suggesting that the method may produce the least contamination. Of objects that meet all three radio loudness criteria, 11.4 per cent are identified as having multiple components, whereas it is only 0.016 per cent for sources meeting none. 1.75 per cent of objects that meet the radio luminosity criteria but not the classical radio loudness cut (i.e. are in the high L_{3000} 'wedge' section of Fig. 2) have multiple components, and 0.47 per cent of those meeting the classical radio loudness but not radio luminosity cuts (i.e. in the lower L_{3000} wedge) have multiple components.

Throughout the rest of the paper, we present the results from the GMM-defined populations as standard, as the approach is data-driven and agnostic to the expected populations, and most efficiently retrieves the multicomponent sources. Using the GMM also allows us to assign classification likelihoods to sources, allowing us to fold uncertainty in classification into our analyses. The results from the other two cuts are presented in Appendix A. In summary, the overall conclusions do not change between classification method, although the connection between L_{3000} and black hole mass results in the weakening of some trends when making a cut in L_{144} alone. All sources that are classified as RL by any method are detected in the original LoTSS DR2 catalogue, and thus do not rely on fluxes derived from forced photometry.

2.3 Population matching

One of the principal aims of this paper is to understand how the presence of a jet is linked to other outflow and accretion properties in quasars. One test is the comparison of the emission line characteristics of our RL/RQ populations, such as C IV blueshift, $\mathrm{EW_{C\ IV}}$ and $\mathrm{EW_{He\ II}}$. In the LoTSS DR1 sample, A. L. Rankine et al. (2021) show that RL quasars systemically display lower C IV blueshifts than RQ ones. However, G. T. Richards et al. (2011) demonstrated that C IV blueshift increases with an increasing luminosity. As RL sources will inherently have a lower optical luminosity at a given radio luminosity than RQ, it is therefore possible that the weaker blueshifts are an artifact of the underlying trend. Alternatively, previous works have found evidence to suggest that RL quasars are generally associated with more massive central black holes (e.g. A. Laor 2000; R. J. McLure & M. J. Jarvis 2004; R. B. Metcalf & M. Magliocchetti 2006; A. Chakraborty & A. Bhattacharjee 2021). It has also been suggested (for example,

by M. Giustini & D. Proga 2019; J. W. Petley et al. 2024) that there is a link between accretion rate and quasar jets, specifically, that a lower accretion rate is expected in the regime where jets dominate over winds. A connection has also been found between accretion rate and C IV blueshift by H. Wang et al. (2011) and J. W. Sulentic et al. (2017), which was extended to two dimensions by M. J. Temple et al. (2023), showing that C IV blueshift is endemic only for the most massive, highly accreting black holes. For EWs, there is the well-known Baldwin effect that leads one to expect weaker C IV and He II in the sources more luminous in the ultraviolet, which is seen in M. J. Temple et al. (2023) to result in deficiencies in these quantities for the most massive, highly accreting black holes also. A. L. Rankine et al. (2021) equally shows that there is stronger overall He II emission in RL quasars.

Overall, it is clear that there is a complex interplay of characteristics that could lead to perceived correlations between emission line and radio properties, primarily related to differences in black hole mass and accretion rate distributions, or, equivalently, luminosity. Any relationships in this space need to be carefully examined to ensure they are not artificially induced, nor driven by underlying correlations in properties unrelated to the question at hand. M. Stepney et al. (2023) use population matching for their sample of SDSS DR16 quasars at $1.5 < z < 4$ to explore the evolution of their ultraviolet emission line properties with redshift. They examine the dependence on ultraviolet luminosity, or both black hole mass and Eddington-scaled accretion rate, and find that differences in C IV blueshifts between different redshift bins can be fully explained by different distributions in luminosities between the populations, as these trends vanish once the matching has taken place. As such, for the populations in our study, if there are observable trends or differences in emission line properties that persist after the matching, we can be sure they are not driven by differences in the black hole masses, Eddington fraction, or L_{3000} of RL and RQ quasars.

We therefore match our RL and RQ populations in L_{3000} and $\mathrm{FWHM_{Mg\ II}}$ space, as these are the fundamental observed quantities that are used to derive the Eddington fraction and black hole mass of the sources. The matching serves equally well to match them in those quantities, too. We perform a two-dimensional (2D) K-nearest neighbours matching procedure using the `NearestNeighbours` function from SCIKIT LEARN with $k = 1$, i.e. a single RQ neighbour returned. None of the RL sources are removed, and some of them share a nearest neighbour RQ source, resulting in 1976 RQ and 2014 RL quasars in the matched sample. In Fig. 3, we show the distribution of RL and RQ sources (as defined by the GMM) in L_{3000} and $\mathrm{FWHM_{Mg\ II}}$ before and after matching. To verify the quality of the match, we carry out a 2D Kolmogorov–Smirnov (KS) test from SCIPY (P. Virtanen et al. 2020). The original distribution has a p-value of 10^{-19}, where anything <0.05 allows us to reject the null hypothesis that the distributions are drawn from the same parent population at the 95 per cent confidence level. After matching, the p-value is 1.0 indicating statistically similar 2D distributions. The redshift distributions of our RL and RQ populations are virtually indistinguishable both before and after matching.

3 RESULTS

3.1 Emission line properties of RL and RQ sources

In this section, we use the matched populations of RL and RQ quasars in various emission line spaces to investigate the differences between the outflows and accretion disc properties of these two populations, decoupled from effects of black hole mass and optical luminosity.

In fig. 7 of G. T. Richards et al. (2011), they compare the blueshift of the C IV emission line to its EW, finding that there are no quasars with both a strong C IV line and large blueshift. They also find, using 1.4 GHz radio data from FIRST (Faint Images of the Radio Sky at Twenty-Centimeters, R. H. Becker, R. L. White & D. J. Helfand 1995), that RL quasars do not occupy a separate part of the parameter space to RQ quasars, although they are more often found at the weaker blueshift part of the regime. A similar plot is reproduced in fig. 5 of A. L. Rankine et al. (2021) using LoTSS DR1, with the same conclusions. We now conduct the same exercise with the larger LoTSS DR2 sample in Fig. 4, both for the whole sample and then for the populations matched in L_{3000} and $\mathrm{FWHM_{Mg\ II}}$.

The overall C IV emission properties are, unsurprisingly, similar to those found by G. T. Richards et al. (2011) and A. L. Rankine et al. (2020, 2021): sources can either have strong C IV emission or strong blueshifts, but not both.[2] And whilst it is possible to find a RL source across the same range of C IV emission space that one might find a RQ quasar, they are concentrated overall at lower blueshifts. Furthermore, even with the populations matched in L_{3000} and $\mathrm{FWHM_{Mg\ II}}$, RL quasars have generally lower C IV blueshifts than their RQ counterparts. The KS test p-values for the unmatched and matched C IV blueshift distributions are 10^{-51} and 10^{-11}, respectively.

On a source-by-source basis, effects such as inclination, and the impact of a constant bolometric correction and scatter in the relationships used to estimate black hole mass and Eddington fraction, act to confound any potential comparisons. However, given that these trends are statistically significant at a population level, the result is important: given the matching procedure, differences in the emission line properties of the populations must be driven by some process unconnected to black hole mass or Eddington fraction. There is also a small remaining difference in the $\mathrm{EW_{C\ IV}}$ of the two populations, which, given that they are well-matched in ultraviolet luminosity, suggests that there is a slightly different Baldwin effect in RL quasars as compared to RQ. When unmatched, the RL and RQ populations have a one-dimensional $\mathrm{EW_{C\ IV}}$ KS test p-value of 10^{-19}, and which becomes 2×10^{-4} when matched in L_{3000} and Mg II. In both cases, the RL and RQ populations are therefore statistically unlikely to be drawn from the same parent distribution.

In Fig. 5, we plot EW versus luminosity for the two ultraviolet lines measured for our sample, He II and C IV. The RL and RQ sources display a Baldwin effect in both lines, which is to say there is a general decrease in EW with increasing luminosity, as shown previously in G. T. Richards et al. (2011) for their sample of SDSS quasars with associated FIRST radio fluxes. However, for both emission lines, despite the populations being effectively matched in black hole mass and Eddington fraction, there is an offset between RL and RQ sources. For a given ultraviolet luminosity, a RL quasar will generally have a stronger He II and C IV line than its RQ counterpart.

[2]As explained in section 4.3 of A. L. Rankine et al. (2021), many of the small number of objects in the lower-left region of Fig. 4 possess unreliable measurements and have deliberately been excluded from the analysis.

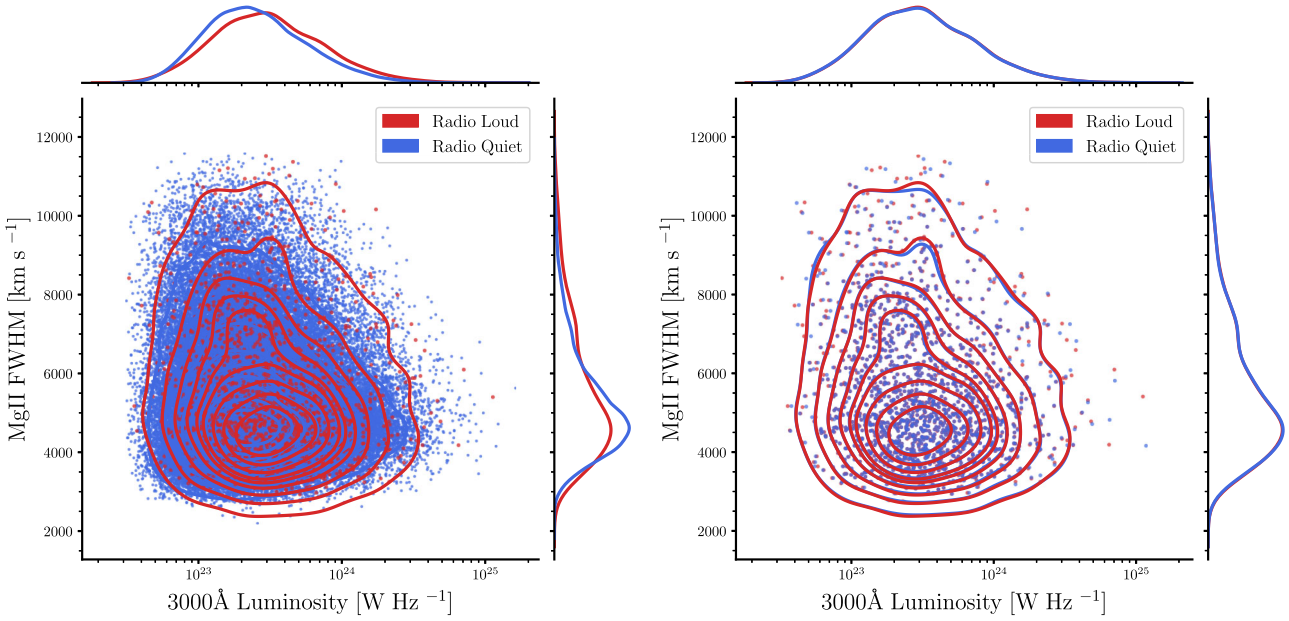

Figure 3. Distributions of radio loud (red points/contours) and radio quiet (blue points/contours) quasars in L_{3000} and FWHM$_{\rm Mg\ II}$ space, for the entire sample (left) and then after NearestNeighbour matching in this space (right). The RL and RQ populations are as defined by the GMM. The matching procedure has removed any differences in these distributions.

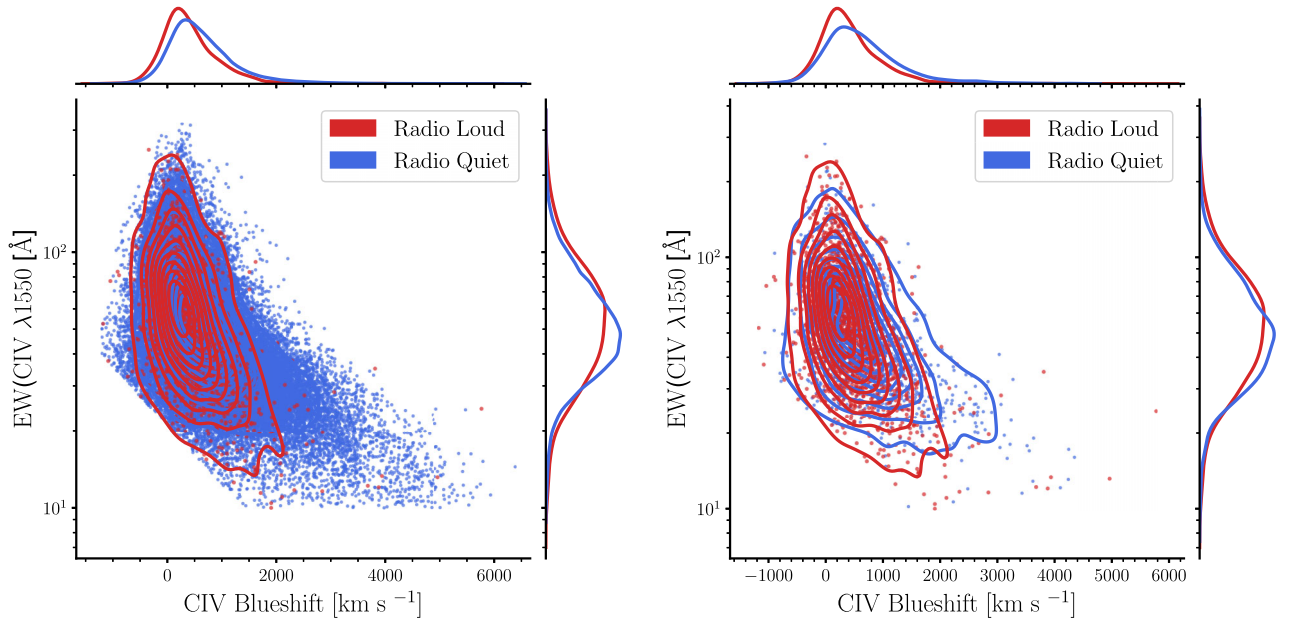

Figure 4. The C IV blueshift and EW$_{\rm C\ IV}$ distributions for radio loud (red points/contours) and radio quiet (blue points/contours) quasars, as defined by the GMM. Similarly to Fig. 3, the left plot is for the entire sample, and the right shows the distribution of sources after they are matched in L_{3000} and FWHM$_{\rm Mg\ II}$. There are clearly differences in both distributions, even after effectively accounting for black hole mass and Eddington fraction.

To investigate the root cause of differences in C IV blueshift between the RL and RQ populations, we carry out a three-dimensional match, now in FWHM$_{\rm Mg\,II}$, L_{3000}, and EW$_{\rm He\ II}$, with corresponding KS test p-values of 0.999 in each variable after matching. As such, the two samples are equivalent in black hole mass, Eddington fraction, and strength of ionizing SED. We test the difference in C IV blueshifts in Fig. 6. The distributions of C IV blueshift post-matching are more similar, but still RQ quasars have slightly higher blueshifts overall. The resulting KS test p-value is 10^{-7}, which suggests that, whilst the difference in strength of the ionising extreme ultraviolet and/or soft X-ray flux between RL and RQ sources is a large factor causing the difference in disc wind speeds, it cannot explain it in its entirety.

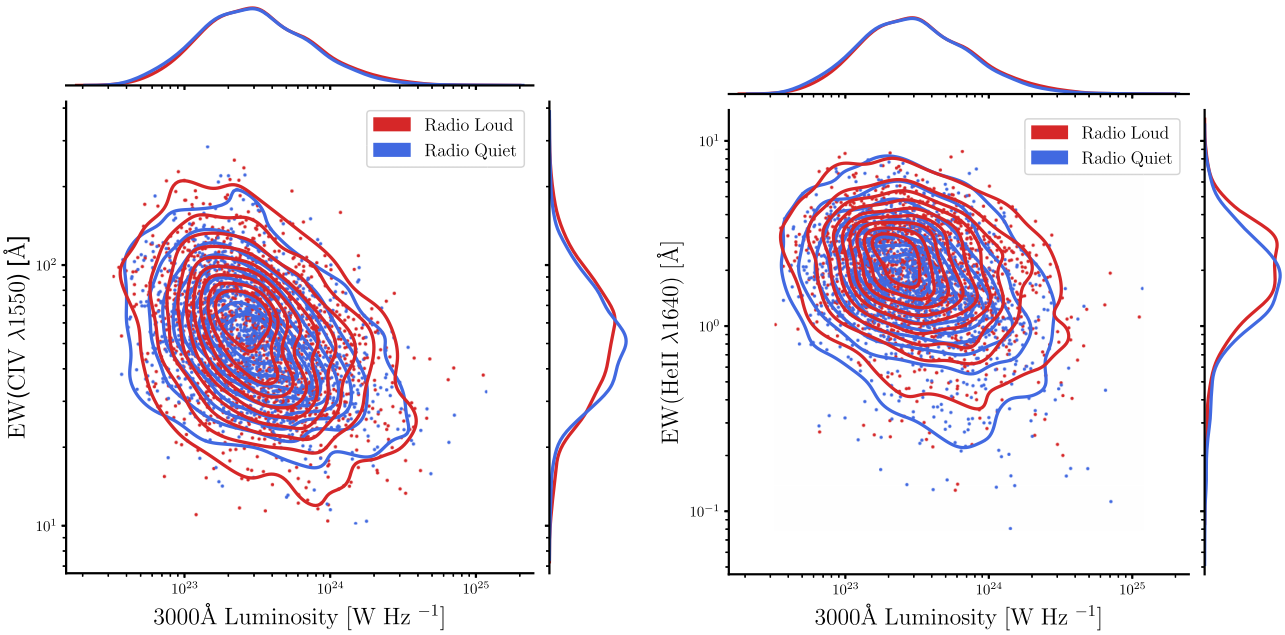

Figure 5. Distribution of radio loud (red points/contours) and radio quiet (blue points/contours) quasars in L_{3000} and the EW of ultraviolet emission lines, C IV (left) and He II (right), for populations matched in L_{3000} and FWHM$_{\rm Mg\ II}$. The RL and RQ populations here are defined by the GMM.

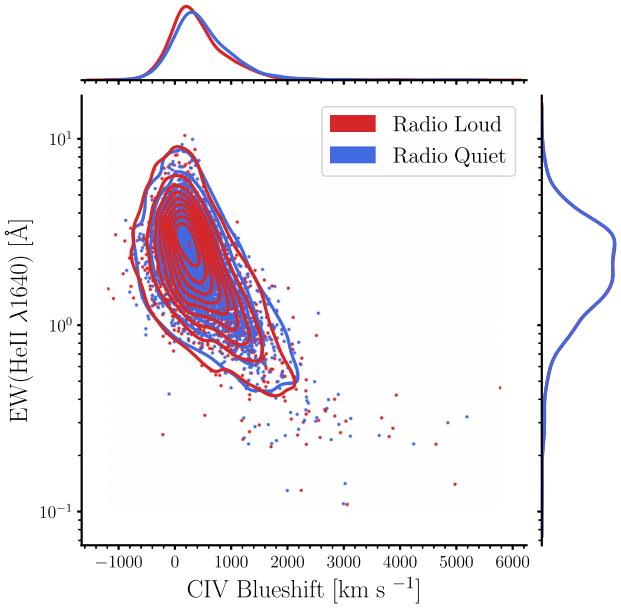

Figure 6. Distribution of C IV blueshift and EW$_{\rm He\ II}$, for radio loud (red points/contours) and radio quiet (blue points/contours) quasars as defined by the GMM, after the populations have been matched in L_{3000}, FWHM$_{\rm Mg\ II}$, and EW$_{\rm He\ II}$. The EW$_{\rm He\ II}$ distribution is well-matched, and the radio loud and quiet populations show greater similarity in C IV blueshift than in Fig. 4, but the radio loud sources are still shifted to lower blueshifts, overall.

There are other very clear differences between the RL and RQ populations when matched in black hole mass and Eddington fraction, demonstrated in Fig. 7. The figure shows how EW$_{\rm C\ IV}$, C IV blueshift, and EW$_{\rm He\ II}$ vary across Eddington fraction and black hole mass space for both RL and RQ sources. The difference is again most prominent for C IV blueshift, where the 'wedge' shape of very high blueshift at the highest black hole masses and Eddington fractions found in M. J. Temple et al. (2023) is significantly weaker for RL sources compared to their RQ counterparts, although there is also significantly weaker He II emission for the RQ sources in this region, too. There is a minor increase in the C IV blueshift and a minor decrease in EW$_{\rm He\ II}$ for the most massive, highly accreting RLs only.

As shown by M. J. Temple et al. (2023), there is an interesting change in EW$_{\rm He\ II}$ behaviour at $(\lambda_{\rm Edd}) \approx 0.1$. In Fig. 7, we show that the change occurs for both RL and RQ sources, albeit with the minimum value (EW$_{\rm He\ II} \sim 1$ Å) only reached by RQ quasars, and a less significant appearance in RL quasars. In the wedge region defined in C IV blueshift, RQ quasars show a clear deficit in He II, inline with the idea that the sources with the weakest ionizing SED are able to drive the strongest disc winds. There is a very similar distribution of EW$_{\rm C\ IV}$ across the entire space for both populations, suggesting whatever is driving the EWs of ~ 100Å $\lambda_{\rm Edd} \lesssim 0.1$, versus the weakest emission, ~ 20 Å, at $\lambda_{\rm Edd} \approx 0.1$ and $M_{\rm BH} > 10^9 {\rm M}_\odot$, is common across both RL and RQ sources. It is also evident that the correlations between the three emission line properties hold true for both sub-populations: that is, for the highest C IV blueshifts, there is also the strongest He II emission line, and the weakest C IV line, and vice versa. These constant correlations suggest there are enough similarities in the BLR of RL and RQ quasars that the coupling of the He II and C IV emission lines is physically consistent. Equally, it is implying that the connection between disc winds and the underlying SED is constant in both RL and RQ sources, as these emission lines act as their tracers, perhaps meaning that differences in one are caused by a different distribution of the other.[3]

[3]See Fig. A6 for the impact caused by a $\log_{10}(R)$ and radio luminosity cut. In summary, the trends are unchanged for the populations defined using a constant radio-loudness cut; however, for the radio luminosity defined

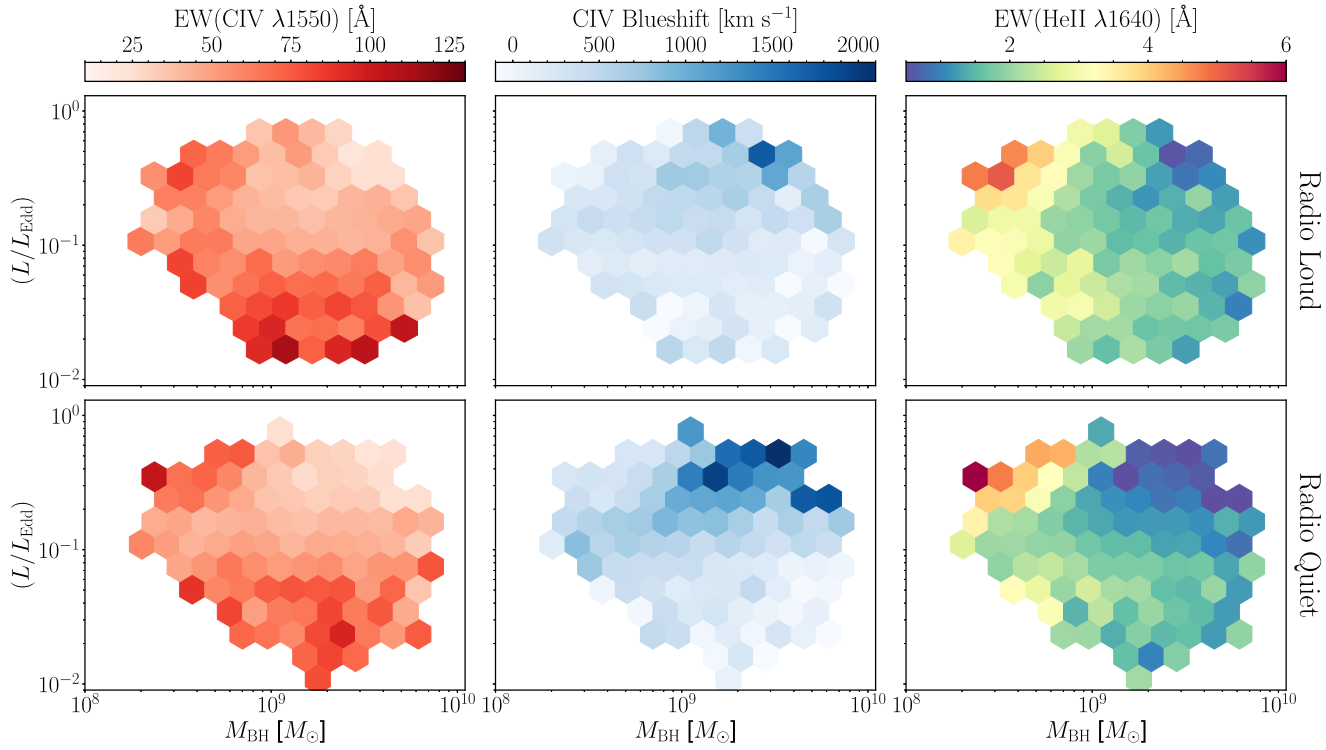

Figure 7. Emission line properties for the matched samples of radio-loud (top row) and radio-quiet (bottom row) quasars in bins of black hole mass and Eddington fraction space. The colour scales show, from left to right, the median value of $EW_{C\ IV}$, C IV blueshift, and $EW_{He\ II}$. The known anticorrelation between C IV blueshift and both He II and $EW_{C\ IV}$ holds for both radio-loud and radio-quiet sources. The trend of high blueshift objects at high black hole masses and Eddington fractions present in radio-quiet sources is not present for radio-loud quasars. The weakest $EW_{He\ II}$ are seen in the same radio-quiet sources with very large black hole masses and Eddington fractions that have high C IV blueshifts.

3.2 Accretion properties of RL and RQ sources

As previously mentioned, it has been suggested by M. Giustini & D. Proga (2019) and J. W. Petley et al. (2024) that the dominant form of outflow mechanism, and thus potentially also the source of radio emission, may be expected to vary with increasing accretion rate, transitioning from being jet-dominated to wind-dominated. In this framework, radio loudness decreases as a function of accretion rate. To test whether we observe such a trend, we show the RL fraction of objects as a function of λ_{Edd}, given by

$$\mathrm{RLfraction} = \frac{N_{RL}}{N_{RL} + N_{RQ}}, \tag{5}$$

where the fraction and numbers are defined within a given bin. In Fig. 8, we utilize the probability of each object being assigned to each GMM cluster, in order to mitigate the effects of uncertainties around borderline sources. As a result, the RL fraction is actually

$$\mathrm{RLfraction} = \frac{\sum_i P_{RL,i}}{N_{RL} + N_{RQ}}, \tag{6}$$

where the sum is over all sources in the relevant bin, and $P_{x,i}$ is the probability of a source i belonging to sample x. At Eddington fractions below $\lambda_{Edd} \sim 0.1$, the fraction of RL sources decreases with increasing accretion rate. However, at $\lambda_{Edd} = 0.1$ the RL fraction reaches a minimum – interestingly, the same point at which M.

ones, there is more of a similarity between RL and RQ properties at high black hole masses and Eddington fractions. A more lenient cut in this part of the parameter space has likely resulted to contamination from objects with intermediate $\log_{10}(R)$ values.

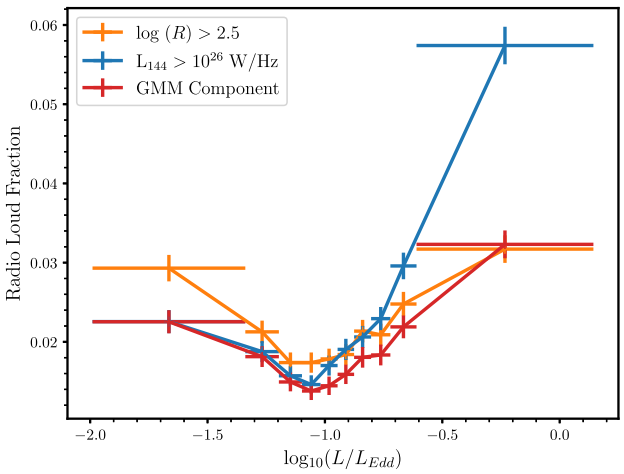

Figure 8. Radio-loud fraction as a function of Eddington fraction, in bins of equal number of objects is shown for each of the three methods of radio loud classification: traditional radio loudness cut (orange), radio luminosity threshold (blue), and GMM component fit (red). All three methods show qualitatively the same trend: an initial decrease, followed by a minimum at 10 per cent of Eddington, then a further increase to a maximum at around the Eddington limit.

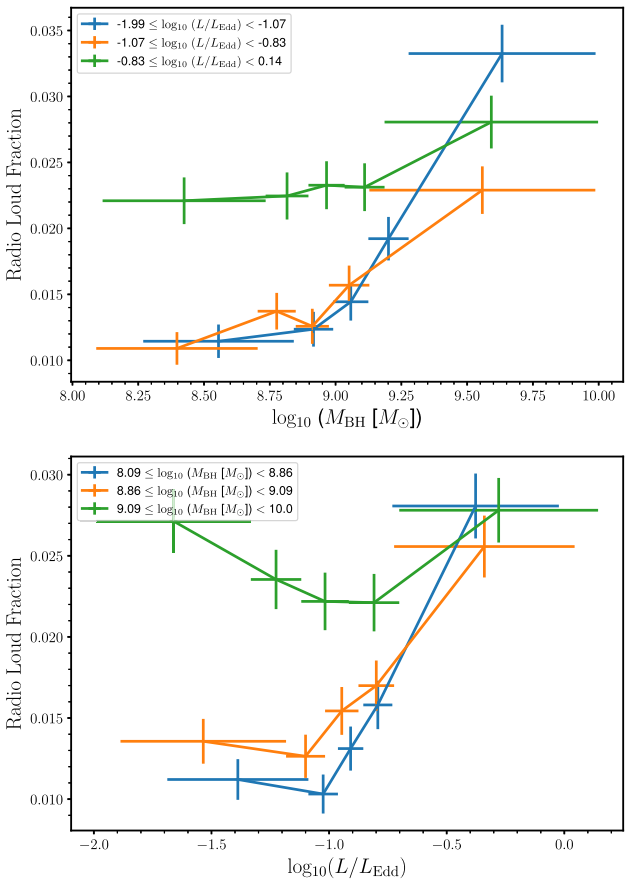

Figure 9. The fraction of objects categorized as radio loud by the GMM as a function of black hole mass (top) and Eddington fraction (bottom). Both are split into bins of equal number of objects, and each line represents varying Eddington fraction (top) or black hole mass (bottom), from lowest (blue) to highest (green). In both cases, low and intermediate bins of one property show a sharp upturn as the other property increases, whereas the highest bins are relatively high throughout.

J. Temple et al. (2023) suggest there is a fundamental change in either BLR or accretion disc properties. Above $\lambda_{\rm Edd} = 0.1$, the RL fraction then increases to a maximum at $\lambda_{\rm Edd} \approx 1$. The peak in RL fraction implies that powerful radio emission is most efficiently produced in quasars with Eddington fractions above $\lambda_{\rm Edd} \approx 0.1$. It has also been verified that these trends do not vary across the range of redshift in our sample.[4]

The investigation of the distribution of RL fraction is expanded in Fig. 9 to examine its dependence on both $\lambda_{\rm Edd}$ and black hole mass, which spans a range of 10^{8-10}M$_\odot$ in our sample. There is a general increase in RL fraction with black hole mass, although the trend becomes shallower with increasing $\lambda_{\rm Edd}$. For $\lambda_{\rm Edd} < 0.15$, the range of RL fraction varies between only 2.2 ± 0.2 and 2.8 ± 0.2 per cent, compared to 1.1 ± 0.1 and 3.3 ± 0.2percnt for $\lambda_{\rm Edd} > 0.085$. The RL fraction associated with the highest $\lambda_{\rm Edd}$ bin is significantly greater than for the other bins for black hole masses $M_{\rm BH} \lesssim 10^{9.45}M_\odot$, above which it is overtaken by the lowest $\lambda_{\rm Edd}$ bin.

In terms of $\lambda_{\rm Edd}$, there is again a clear distinction between objects with the highest and lowest black hole masses. It is clear that above $\lambda_{\rm Edd} < 0.1$ in Fig. 8, the RL fraction is dominated by the highest mass objects. In fact, in the highest black hole mass bin the RL fraction is ~ 2.5 times higher than in those with intermediate mass black holes ($M_{\rm BH} \lesssim 10^9$M$_\odot$) when $\lambda_{\rm Edd} < 0.1$, at values of 2.7 ± 0.2 per cent versus 1.1 ± 0.1per cent, respectively.

When $\lambda_{\rm Edd} > 0.3$, RL fraction is comparable for all black hole masses, at ≈2.7 per cent. Generally, there is an increasing RL fraction with increasing $\lambda_{\rm Edd}$, particularly when the black hole mass $M_{\rm BH} \lesssim 10^9$M$_\odot$. At masses $M_{\rm BH} \gtrsim 10^9$M$_\odot$, there is a high RL fraction across the entire $\lambda_{\rm Edd}$ range.

Fig. 10 demonstrates in greater detail the origins of these trends, showing the 2D distribution of RL fraction across Eddington fraction and black hole mass for all three classification methods. There is a high RL fraction of ∼5–10 per cent at $\lambda_{\rm Edd} \geq 0.3$, and again at black hole masses of $M_{\rm BH} > 10^{9.4}$M$_\odot$. Intriguingly, when *both* of these criteria are met, the RL fraction is not always high; specifically, for the left and right hand panels, the extreme upper right-corner of the parameter space displays a typical RL fraction lower than the maximum value. The observed distribution can either be interpreted as the presence of two distinct regions of relatively high RL fraction, one at high $\lambda_{\rm Edd}$ and the other at high black hole mass, or alternatively that there is some suppression of jet formation in the quasars with the most massive, highly accreting black holes. In Section 4.2, we discuss both possible interpretations. However, when we use a radio luminosity cut (right-hand panel of Fig. 10) the reduction at high $\lambda_{\rm Edd}$ and high black hole mass vanishes, and instead, there is a constant RL fraction of >8 per cent wherever the $\lambda_{\rm Edd} > 0.3$ or $M_{\rm BH} > 10^{9.4}$M$_\odot$ criteria are met. Interestingly, the region of reduced RL fraction in the GMM and radio loudness defined distributions corresponds remarkably well with the 'wedge' of high C IV blueshift, defined in M. J. Temple et al. (2023) and Fig. 7.

Combined, Figs 9 and 10 paint a compelling picture: RL fraction (and thus, inferred jet production) can be increased by a high accretion rate (as inferred from $\lambda_{\rm Edd}$) or a high black hole mass, and these two properties do not act in isolation, but are influenced by each other.

4 DISCUSSION

Here, we consider the possible physical interpretations of our results and the implications of the different radio loud classification methods used in this paper. For the purposes of this discussion, we assume that the observational tracers of jets, disc winds, SED, and accretion rate (i.e. whether a source is radio loud, the blueshift of its C IV emission line, the EW$_{\rm He\ II}$, and $\lambda_{\rm Edd}$, respectively) act as reasonably accurate indicators of these properties, at least at a population level.

4.1 Implications of different classification methods

For the majority of our results, the main conclusions are insensitive to the choice of RL classification method. The main difference between the samples produced by the three methods is that many more objects are classified as RL using the radio luminosity

[4]These trends are consistent across the three methods, the main difference occurring at Eddington fractions of the order of unity, where a cut in radio luminosity shows a RL fraction of nearly 5.7 ± 0.2 per cent, compared to the 3.2 ± 0.2 per cent for the other two methods.

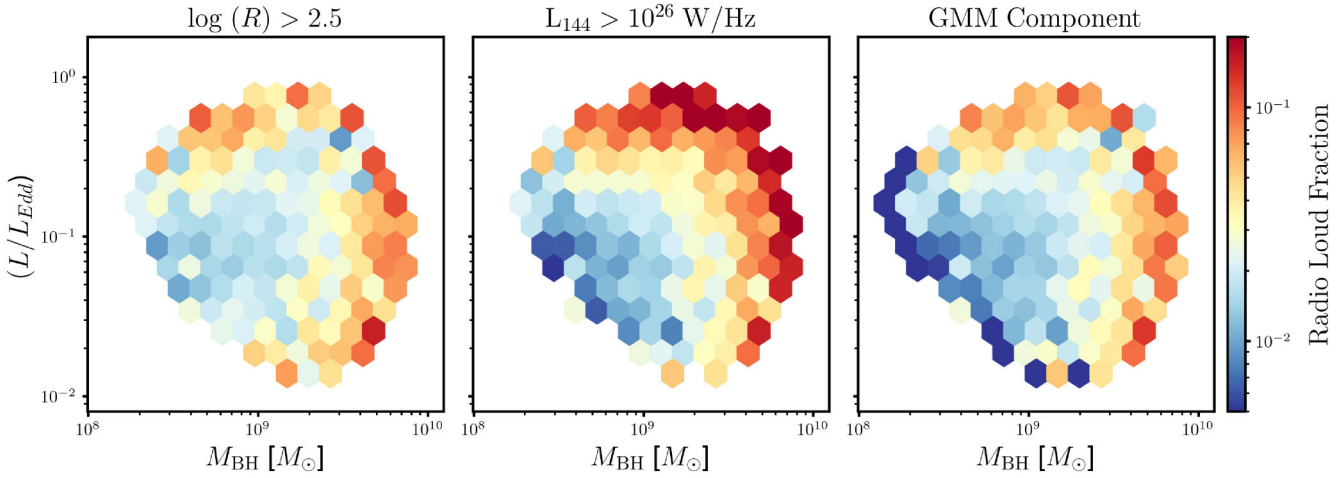

Figure 10. The distribution of average (mean) radio loud fraction in bins of black hole mass and Eddington fraction space, coloured on a log scale. The three panels show the results of the three different radio loud classification methods: classical radio loudness cut (left), GMM component assignment (middle) and radio luminosity threshold (right). The main difference here is the presence of many more radio loud sources with high black hole masses and Eddington fractions in the luminosity cut plot, driven by sources that are otherwise classified as radio quiet but have very high absolute radio luminosities.

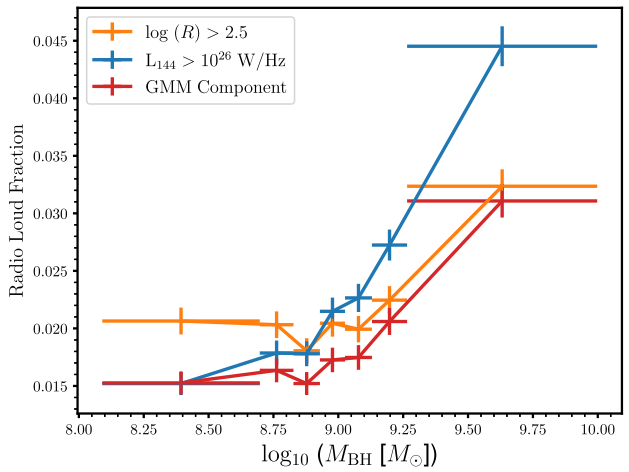

Figure 11. The fraction of quasars that are classified as radio loud, in bins of black hole mass with equal populations. The results are the same if the sample is binned using equal widths but different numbers. Results using the three different classifications methods are shown, with traditional radio loudness cut (orange), radio luminosity threshold (blue), and GMM component fit (red). The fraction is relatively constant for the radio loudness cut and the GMM until black hole masses of $\sim 10^{9.2}$M$_\odot$, whereas the luminosity cut threshold shows a steady increase across the entire range of masses.

classification than the other two methods, particularly for sources that also display a large L_{3000}.

The radio luminosity cut inherently biases the RL sample towards the most massive, highly accreting systems that, by definition, will be the most luminous at L_{3000} (e.g. equations 1 and 2). These sources may also produce prodigious radio luminosity from other mechanisms as well as jets (see Section 1.2 for brief overview), meaning that luminous RQ quasars may contaminate the RL sample. However, the results from a constant luminosity cut do also tell us something interesting. In Fig. 2, the upper envelope of the bulk distribution of RQ sources appears to flatten off at $L_{3000} \gtrsim 10^{24} W\ Hz^{-1}$. At these high luminosities, a flatter cut should indeed be used to discriminate jetted/non-jetted objects, and many of the sources identified as RL by the luminosity cut are valid, and the other two methods are missing a substantial fraction. The exclusion of sources in this region could in part explain the 'missing' wedge of sources seen in Fig. 10 at high black hole mass/ Eddington fraction, that is filled in for the luminosity cut defined samples. Indeed, there are examples of traditionally designated 'RQ', very massive sources (e.g. $M_{\rm BH} \approx 10^{9-10}M_\odot$) with powerful radio jets (T. Sbarrato et al. 2021). If the 2D RL fraction distribution from middle panel of Fig. 10 is in fact most representative of the behaviour of AGN jet fraction, then there is no 'missing' wedge, and the situation reverts to the simpler result: jet formation or prevalence is driven by high accretion rate and/or high black hole mass. There is also another interesting implication. For radio luminosity to no longer scale with optical luminosity, the source of radio luminosity (for these powerful RL quasars, relativistic jets) cannot continue to increase with increasing disc size/luminosity. That is, there is a maximum jet power able to be reached by quasars, which would be governed by an upper limit of jet launching efficiency, as suggested by C. A. C. Fernandes et al. (2011) – and some of the most massive and optically luminous quasars in our sample might be hitting it.

However, it is also entirely possible that the simple luminosity cut instead causes the sample to be biased to the most optically luminous systems, that inherently possess large radio luminosities. In Fig. 2, it would appear that this cut does start to include some of sources at the upper edge of the RQ distribution, but if the cut were to be set any higher it would miss sources that are almost certainly *bona fide* RL quasars at the lower end of the optical luminosity range. Inversely, the use of a traditional constant radio loudness cut may have the opposite effect: at $L_{3000} < 10^{23}$ W Hz^{-1}, the radio emission threshold to meet even a strict cut (e.g. $\log_{10}(R) > 2.5$) is such that it is feasible that objects with strong winds or high star formation rates could produce enough radio emission to be classified as RL. To be classified as RL, an object with a higher L_{3000} (e.g. a quasar with a brighter disc)

needs to have a radio luminosity up to two orders of magnitude brighter than one with a fainter disc. Therefore, at at high optical luminosities, the resulting sample from the $\log_{10}(R)$ cut could thus be biased towards only including the most luminous jets, risking losing those with more intermediate luminosities. Equivalently, there would be jetted objects missing from the sample at the highest optical luminosities, and RQ objects erroneously identified as RL at the lowest. By extension, that may mean the true RL fraction for the most massive, accreting objects may be suppressed, or artificially inflated for the smallest, least accreting sources. These potentially 'missing' RL sources at the highest black hole masses and Eddington fractions could contributing to the creation of uncertainty in the upper right hand 'wedge' portion of Fig. 7.

Given all the above, it is preferential to utilize a cut that relaxes the radio luminosity requirement at high optical luminosities, while still enforcing a high enough criteria at the lower end to ensure there is minimal contamination. Fortunately, the GMM classification naturally provides both of these things, as it defines two populations somewhere in-between the other two methods; furthermore, the approach is driven by the data and does not require a subjective choice of threshold. However, it should be noted that if a Bayesian GMM algorithm is used (i.e. one that self-determines the number of components required to describe the distribution), it routinely returns models with ∼30 components. The large number of components is indicative of the fact that the distribution of sources in radio and optical luminosity is *not* a true dichotomy, but instead a continuous distribution. However, for our analysis, we seek a simple way to classify objects into RL and RQ, and the GMM fitting method would appear to be the most reliable, unbiased way of doing so. An additional strength of the GMM method is that it is possible to calculate the probability that a source is in each cluster, which allowed us to use these probabilities instead of a binary classification when calculating properties such as RL fraction (equation 6). Such a statistical classification is undoubtedly preferable in situations when the RL/RQ nature of the source is ambiguous or the data point lies close to the boundary between populations. Returning to the concept of a 'missing wedge' for the highest black hole masses and $\lambda_{\rm Edd}$ (i.e. as described in Section 3.1), its ubiquity, independent of the definition of RL objects, suggests the feature is an intrinsic property of the distribution.

4.2 Physical implications: disc–jet coupling

The connection between accretion rate, black hole mass, and radio loudness in our sample of quasars is somewhat complex. It is clear that quasars are most able to launch jets when they have $M_{\rm BH} > 10^9 {\rm M}_\odot$ or $\lambda_{\rm Edd} > 0.3$, as shown in Figs 9 and 10. However, whilst there is significant uncertainty in the region with the highest black hole masses and Eddington fractions, there is tentative evidence to suggest that quasars with both a high black hole mass and high $\lambda_{\rm Edd}$ are associated with a relatively lower RL fraction. We interpret the RL fraction as the relative prevalence of jetted quasars, or alternatively, the jet launching efficiency of quasars with a given set of properties.

There are perhaps two equivalent ways of considering the result: that accretion rate and black hole mass are two mutually exclusive requirements that correspond to two different jetted populations, or that a high accretion rate and/or black hole mass contributes to jet launching, yet something acts to suppress jet formation for the most extreme sources. Focussing first on the former, we consider how this idea fits with previous studies.

4.2.1 Black hole mass dependence

There has been much attention paid to the connection between black hole mass and radio loudness. For example, R. McLure & J. Dunlop (2001) found that a black hole mass of $M_{\rm BH} > 10^9 {\rm M}_\odot$ is needed to produce a powerful RL quasar, and both M. Lacy et al. (2001) and P. N. Best et al. (2005) find a strong positive correlation between black hole mass and radio emission. R. J. McLure & M. J. Jarvis (2004) also find that RL quasars are host to more massive black holes than RQ quasars. More recently, I. H. Whittam et al. (2022) find in AGN generally, a black hole mass of $M_{\rm BH} > 10^{7.8} {\rm M}_\odot$ is needed to launch and sustain a radio jet with mechanical power greater than the overall radiative output of the AGN, while C. Macfarlane et al. (2021) find a typical jet power that increases with the black hole mass in SDSS quasars. Sabater, J. et al. (2019) also find using cross-matched SDSS DR7 and LoTSS DR1 data that activity in the general radio AGN population (i.e. not limited to quasars) shows a strong positive correlation with black hole mass. The general consensus is that one might expect to find more jetted AGNs at higher black hole masses, and our results support the hypothesis for quasars.

However, B. H. Yue et al. (2025) finds no connection between jet activity and black hole mass for the majority of their sample of SDSS DR16 quasars, apart from with the top 20 per cent most massive black holes. We too see this in our results, such as in Fig. 11, where there is no significant increase in radio loud fraction up to ${\rm M}_{\rm BH} \approx 10^{9.1} {\rm M}_\odot$, which is approximately the 80th mass percentile in our sample. However, the trend is not universal. The radio luminosity defined sample instead shows a general increase with black hole mass across the entire mass range. Furthermore, as seen in Fig. 9, the increase in RL fraction is less pronounced for sources in the highest $\lambda_{\rm Edd}$ bin. The fact that BH mass trends change with Eddington fraction, and vice versa, highlights once again the importance of considering them in combination when trying to understand the nature of quasar jet launching. To summarize, it is clear that regardless of the Eddington fraction, high black hole masses ($M_{\rm BH} > 10^9 {\rm M}_\odot$) drive a high RL fraction, consistent with previous findings of a black hole mass dependence on jet launching. The inverse is also true: a high Eddington fraction ($\lambda_{\rm Edd} \gtrsim 0.1$) is associated with a high RL fraction, independent of black hole mass.

4.2.2 Accretion rate dependence

How does the literature expect accretion rate to link to the launching of jets in quasars? M. Giustini & D. Proga (2019) propose that the dominant source of radio emission in quasars changes with accretion rate, initially jet dominated at very low $\lambda_{\rm Edd}$, until a transition to disc wind domination within systems approaching their Eddington limit. The result is supported by J. W. Petley et al. (2024), who suggest that radio emission across the range of Eddington fractions is generated by different processes, with disc winds at one end and jets at the other, assuming that disc winds produce detectable radio emission. Within the range of Eddington fractions that we observe in our sample, however, we do not see the same effect. We do observe an anticorrelation between radio properties and C IV blueshift, shown in the differences between RL and RQ quasars in Fig. 4, and the co-location of high

C IV blueshift and reduced RL fraction in Figs 7 and 10. However, the highest RL fractions are instead associated with the highest Eddington fractions ($\lambda_{\rm Edd} \gtrsim 0.1$), as seen in Figs 8–10. There are relatively fewer sources overall at high $\lambda_{\rm Edd}$, however, there is a steeper drop-off in RQ sources than RL. That is to say, if a source has a high Eddington fraction, it is more prone to being RL than otherwise, or, by extension, that jet launching efficiency in this region of the parameter space is higher.

Then, the question becomes why might a high Eddington fraction lead to a high jet launching fraction, or efficiency. It can be reasonably expected that accreted matter will carry magnetic flux (M. J. Rees et al. 1982), which can lead to a collimation of matter from the disc and a subsequent massive ejection in the form of a jet, as described by the R. D. Blandford & D. G. Payne (1982) (BP) formalism. Indeed, J. Ferreira et al. (2013) suggest that a BP-driven jet has its power directly controlled by the source's accretion rate, with higher accretion leading to greater jet power. Perhaps, then, the 'accretion rate driven' component of the RL fraction that we are seeing in Fig. 10 may be dominated by disc-launched, BP-like jets. Given that radio-loudness is a ratio and crudely encodes the efficiency of jet production relative to the accretion power, an increase of RL fraction with Eddington ratio may also require an increased jet *efficiency* in the same direction. In a BP-driven jet, this efficiency increase could be achieved through a dependence on the disc aspect ratio (J. Ferreira et al. 2013). Alternatively, within a BZ scenario, a correlation between jet efficiency and Eddington ratio can emerge due to more efficient accumulation of magnetic flux (e.g. A. Ricarte, R. Narayan & B. Curd 2023) or an accretion-rate dependence of BH-spin (see also Section 4.4).

4.3 Physical implications: disc wind–jet connection

The second possible interpretation of the results in Fig. 10 is that there is something preventing the most massive, highly accreting quasars from consistently launching jets in an otherwise continuous distribution of high RL fraction at high Eddington fractions and black hole mass.

It is instructive to consider the differences in emission line properties as shown in Fig. 7. The most striking difference between the matched samples of RQ quasars and RL quasars is clearly the absence of high C IV blueshifts at high $\lambda_{\rm Edd}$ and high black hole mass for RL quasars (Fig. 7). M. J. Temple et al. (2023) found that the most massive, highly accreting quasars typically display the largest C IV blueshifts, which can be interpreted as showing the strongest disc winds. The finding is consistent with work by A. Baskin & A. Laor (2005) and M. Giustini & D. Proga (2019), who suggest that a high $\lambda_{\rm Edd}$ coupled with a high black hole mass is necessary for strong C IV blueshifts if they are produced by disc winds. However, in our results, the need for high $\lambda_{\rm Edd}$ and black hole mass to generate disc winds is only observed for sources that are RQ. One key question is therefore: does the presence of a jet inhibit disc winds, or do strong disc winds in quasars quench jet launching?

The existence of an anticorrelation between jets and disc winds is something that is well documented, both in quasars and in other accreting systems. J. Neilsen & J. C. Lee (2009) find that, in microquasars, winds in the accretion disc can suppress jet activity by carrying away sufficient matter to halt the flow of mass into the jet. Related behaviour can be seen in quasars at the population level: fig. 3 of A. L. Rankine et al. (2021), where it shows that there is a decrease in RL fraction with increasing C IV blueshift, a results supported by fig. 5 of A. L. Rankine et al. (2021), G. T. Richards et al. (2011), and Fig. 4 in this paper. All of these works point to a systemically lower C IV blueshift in RL quasars compared to their RQ counterparts. Further suggestions of a wind–jet anticorrelation or bimodality have been made based on broad absorption line quasar properties (L. K. Morabito et al. 2019; J. W. Petley et al. 2022) and X-ray spectroscopy of radio-loud Seyfert AGN (M. Mehdipour & E. Costantini 2019).

If the accretion disc winds are in fact a result of line driving, then we would expect to find a strong dependence on the ionizing SED (e.g. N. Murray et al. 1995; D. Proga 2000; G. T. Richards et al. 2011; M. Giustini & D. Proga 2019; A. L. Rankine et al. 2021), which would presumably manifest as an (anti)correlation between the strength of C IV blueshift and $\rm EW_{He\ II}$. Indeed, in the region of Fig. 7 where we observe the highest C IV blueshifts in RQ sources, we also see the weakest $\rm EW_{He\ II}$. Low $\rm EW_{He\ II}$ could be indicative of a softer SED, that does not overionize the gas in the disc and instead allows a line-driven wind to occur. The anticorrelation between C IV blueshifts and $\rm EW_{He\ II}$ is not present in the RL sources, which show a comparable $\rm EW_{He\ II}$ across all $\lambda_{\rm Edd}$ for black hole masses $M_{\rm BH} > 10^9 \rm M_\odot$.

The increased ionization from the harder SED in RL sources likely precludes the formation of a disc wind, although there are also RQ sources with low C IV blueshift, so a lack of wind does not itself guarantee efficient jet launching. In Fig. 5, we show that for a given L_{3000}, a RL source will generally have a larger $\rm EW_{He\ II}$. As the RL and RQ quasars are matched in L_{3000} and $\rm FWHM_{Mg\ II}$, and thus effectively black hole mass and Eddington fraction, we find that two otherwise equivalent quasars will have different SEDs, depending on whether or not a radio jet is present, with RL sources possessing a 'harder' ionizing spectrum. In Section 4.4, we discuss a possible cause. The results is consistent with the findings of A. L. Rankine et al. (2021), who found that strong $\rm EW_{He\ II}$ is a necessary but not sufficient condition for a jet to be present in their quasar sample, and that the presence of jets and quasar SED shape are likely to be correlated.

4.4 Black hole spin

In the well-known spin paradigm, a key determining factor of whether or not a quasar will produce a jet is the spin of its central black hole, with jets presumably associated with higher spin. A resulting general relativistic effect is that a quasar with a rapidly spinning black hole will also have an inner disc that extends closer to that black hole, which – depending on the detailed accretion disc and corona physics – could result in an increased EUV flux. Therefore, it is possible that the differences in $\rm EW_{He\ II}$ between high mass, high accretion rate RL and RQ quasars is a result of higher spin in those with jets (see discussion by G. T. Richards et al. 2011; A. L. Rankine et al. 2021). However, whilst the presence of increased spin for sources that possess jets is appealing, there is no general increase in $\rm EW_{He\ II}$ for all RL quasars. The apparent decrease in the probability of jet-formation in sources with high $\lambda_{\rm Edd}$ and high black-hole mass also requires further explanation in this scenario.

Furthermore, although the RL fraction of our sample is highest for $M_{\rm BH} > 10^9 \rm M_\odot$ and $\lambda_{\rm Edd} > 0.3$, it is at most ~ 10 per cent. If rapid spin and a high black hole mass and/or a high accretion rate are necessary and sufficient conditions for efficient jet launching, then this behaviour would indicate that the spin values in the quasars are generally small, or otherwise the RL fraction would be much higher. However, such a scenario goes against popu-

lation synthesis models such as M. Volonteri et al. (2005) and S. L. Shapiro (2005), who both predict that the distributions of black hole spins in accreting systems, including quasars, should be skewed towards maximal. Therefore, either these conditions are insufficient, and instead there is another factor at play (e.g. magnetic field configuration, A. Tchekhovskoy 2015), or that our understanding of black hole spin which allows predictions such as those made by M. Volonteri et al. (2005) and S. L. Shapiro (2005) is incomplete. The reality of which of these scenarios is correct, if either, is beyond the scope of this paper, but is a key issue that still needs to be resolved.

5 CONCLUSIONS

We have used the rich multiwavelength data created by combining the LoTSS DR2 with the sub-set of SDSS DR17 that underwent spectral reconstructions in M. J. Temple et al. (2023), following the method of A. L. Rankine et al. (2020), to investigate the connection between disc winds, radio jets, Eddington fraction, and black hole mass in quasars between $1.5 < z < 2.5$. Our main conclusions are as follows:

(i) We have used a GMM to divide the distribution of sources into 'radio loud' and 'radio quiet' classifications, which is a statistically rigorous and easily reproducible methodology that allows for the incorporation of probabilities of that a source is radio loud/radio quiet. We have compared the results of this method of classification to that of a traditional radio loudness or radio luminosity cut, and have found that they are generally similar (Figs 2, 8, and 10).

(ii) The fraction of sources inferred to be jetted varies non-linearly with Eddington fraction, increasing at low and high Eddington fractions, with a minimum at $\lambda_{\rm Edd} \approx 0.1$ and a characteristic 'U' shape (Fig. 8). This is also the location at which M. J. Temple et al. (2023) suggest a change in the physics of the broad line region, although it is unclear if these two results are directly connected. The radio-loud fraction is also greatest for sources with the highest Eddington fractions, $\lambda_{\rm Edd} \approx 0.3$.

(iii) For efficient jet launching, i.e. for a relatively large fraction of the sources to be presumed to possess a jet, quasars in our sample require either $M_{\rm BH} > 10^9 {\rm M}_\odot$ or $\lambda_{\rm Edd} > 0.3$ (Figs 10 and 9). This result is consistent with the idea that more massive black holes are able to generate more powerful radio emission, however it also hints towards an accretion-driven jet formation mechanism. We also find that the most massive, highly accreting quasars appear to less consistently form jets than those which are only massive, or highly accreting.

(iv) In agreement with A. L. Rankine et al. (2021), we find that radio loud quasars generally have weaker C IV blueshifts than radio quiet quasars, which we interpret as corresponding to weaker disc wind velocities. We now confirm that this result holds even when accounting for black hole mass, Eddington fraction (Figs 4 and 7) and the strength of the ionizing SED (Fig. 6). The difference between populations is particularly clear for very massive, highly accreting sources ($\lambda_{\rm Edd} > 0.3$, $M_{\rm BH} > 10^9 {\rm M}_\odot$). We infer that there is an anticorrelation between the strength of accretion disc winds and the efficiency of jet launching, although weak wind signatures do not guarantee a high radio-loud fraction.

(v) We find a different Baldwin effect in radio-loud and radio-quiet quasars, in both $\rm EW_{C\ IV}$ and $\rm EW_{He\ II}$, although it is most pronounced in the latter. Thus, for a given L_{3000}, black hole mass, and Eddington fraction, a radio loud quasar will have a stronger C IV and He II line than its RQ counterpart, and therefore a 'harder' SED. Similar to the case for the C IV blueshifts, these differences are particularly strong for sources with $\lambda_{\rm Edd} > 0.3$ and $M_{\rm BH} > 10^9 {\rm M}_\odot$. The differences in SED between the two populations may be a result of the radio-loud sources having generally more rapidly spinning central black holes, as per the well-known spin paradigm.

ACKNOWLEDGEMENTS

CLJ and JHM acknowledge funding from a Royal Society University Research Fellowship (URF\R1\221062). CLJ gratefully acknowledges support from the Balliol College Dervorguilla Scholarship. We thank Micah Bowles and Sophie Jewell for useful suggestions, and also thank Gordon Richards, Bohan Yue, Leah Morabito and Nicholas Choustikov for insightful discussions. We also extend our thanks to the anonymous reviewer for their feedback and suggestions. IHW and MJJ acknowledge support from the Oxford Hintze Centre for Astrophysical Surveys which is funded through generous support from the Hintze Family Charitable Foundation. MJJ acknowledges support from a United Kingdom Research and Innovation (UKRI) Frontiers Research Grant (EP/X026639/1), which was selected by the European Research Council. MJT acknowledges funding from UKRI grant ST/X001075/1. ALR acknowledges support from a Leverhulme Early Career Fellowship. This work made use of ASTROPY (Astropy Collaboration 2013, 2018, 2022), SEABORN (M. L. Waskom 2021), MATPLOTLIB (C. R. Harris et al. 2020), SCIKIT-LEARN (F. Pedregosa et al. 2011), SCIPY (P. Virtanen et al. 2020), and NUMPY (C. R. Harris et al. 2020).

LOFAR data products were provided by the LOFAR Surveys Key Science project (LSKSP; https://LOFAR-surveys.org/) and were derived from observations with the International LOFAR Telescope (ILT). LOFAR (M. P. Haarlem et al. 2013) is the Low Frequency Array designed and constructed by ASTRON. It has observing, data processing, and data storage facilities in several countries, which are owned by various parties (each with their own funding sources), and which are collectively operated by the ILT foundation under a joint scientific policy. The efforts of the LSKSP have benefited from funding from the European Research Council, NOVA, NWO, CNRS-INSU, the SURF Co-operative, the UK Science and Technology Funding Council, and the Jülich Supercomputing Centre.

Funding for the Sloan Digital Sky Survey IV has been provided by the Alfred P. Sloan Foundation, the U.S. Department of Energy Office of Science, and the Participating Institutions. SDSS-IV acknowledges support and resources from the Center for High Performance Computing at the University of Utah. The SDSS website is www.sdss.org.

SDSS-IV is managed by the Astrophysical Research Consortium for the Participating Institutions of the SDSS Collaboration including the Brazilian Participation Group, the Carnegie Institution for Science, Carnegie Mellon University, Harvard-Smithsonian Center for Astrophysics, the Chilean Participation Group, the French Participation Group, Instituto de Astrofísica de Canarias, The Johns Hopkins University, Kavli Institute for the Physics and Mathematics of the Universe (IPMU)/University of Tokyo, the Korean Participation Group, Lawrence Berkeley National Laboratory, Leibniz Institut für Astrophysik Potsdam (AIP), Max-Planck-Institut für Astronomie (MPIA Heidelberg), Max-Planck-Institut für Astrophysik (MPA Garching),

Max-Planck-Institut für Extraterrestrische Physik (MPE), National Astronomical Observatories of China, New Mexico State University, New York University, University of Notre Dame, Observatário Nacional/ MCTI, The Ohio State University, Pennsylvania State University, Shanghai Astronomical Observatory, United Kingdom Participation Group, Universidad Nacional Autónoma de México, University of Arizona, University of Colorado Boulder, University of Oxford, University of Portsmouth, University of Utah, University of Virginia, University of Washington, University of Wisconsin, Vanderbilt University, and Yale University.

DATA AVAILABILITY

The data underlying this article were accessed from the Sloan Digital Sky Survey (https://www.sdss4.org/dr17/) and the LOFAR Two-metre Sky Survey (https://LOFAR-surveys.org/dr2_release.html). The derived data generated in this research will be shared on reasonable request to the corresponding author.

REFERENCES

Abdurro'uf et al., 2022, ApJS, 259, 35
Astropy Collaboration 2013, A&A, 558, A33
Astropy Collaboration 2018, AJ, 156, 123
Astropy Collaboration 2022, ApJ, 935, 167
Baldwin J. A., 1977, ApJ, 214, 679
Baloković M., Smolčić V., Ivezić Ž., Zamorani G., Schinnerer E., Kelly B. C., 2012, ApJ, 759, 30
Baskin A., Laor A., 2005, MNRAS, 356, 1029
Baskin A., Laor A., Hamann F., 2013, MNRAS, 432, 1525
Beaklini P. P. B., Quadros A. V. C., de Avellar M. G. B., Dantas M. L. L., Cançado A. L. F., 2020, MNRAS, 497, 1463
Becker R. H., White R. L., Helfand D. J., 1995, ApJ, 450, 559
Beckmann V., Shrader C. R., 2012, Active Galactic Nuclei, Wiley-VCH Verlag GmbH, Weinheim, Germany, p. 380
Begelman M. C., McKee C. F., Shields G. A., 1983, ApJ, 271, 70
Best P. N., 2007, New Astron. Rev., 51, 168
Best P. N., Kauffmann G., Heckman T. M., Brinchmann J., Charlot S., Ivezić Ž., White S. D. M., 2005, MNRAS, 362, 25
Bicknell G. V., 2002, New Astron. Rev., 46, 365
Blandford R. D., Payne D. G., 1982, MNRAS, 199, 883
Blandford R. D., Znajek R. L., 1977, MNRAS, 179, 433
Bonzini M. et al., 2015, MNRAS, 453, 1079
Broderick J. W., Fender R. P., 2011, MNRAS, 417, 184
Calistro Rivera G. et al., 2017, MNRAS, 469, 3468
Calistro Rivera G. et al., 2024, A&A, 691, A191
Castor J. I., Abbott D. C., Klein R. I., 1975, ApJ, 195, 157
Chakraborty A., Bhattacharjee A., 2021, Astron. Nachr., 342, 142
Cirasuolo M., Celotti A., Magliocchetti M., Danese L., 2003, MNRAS, 346, 447
Condon J. J., 1992, ARA&A, 30, 575
Condon J. J., O'Dell S. L., Puschell J. J., Stein W. A., 1980, Nature, 283, 357
Elvis M. et al., 1994, ApJS, 95, 1
Everett J. E., Ballantyne D. R., 2004, ApJ, 615, L13
Fawcett V. A., Alexander D. M., Rosario D. J., Klindt L., Fotopoulou S., Lusso E., Morabito L. K., Calistro Rivera G., 2020, MNRAS, 494, 4802
Fawcett V. A. et al., 2023, MNRAS, 525, 5575
Fernandes C. A. C. et al., 2011, MNRAS, 411, 1909
Ferreira J., Petrucci P.-O., Garnier Q., 2013, in Gómez J. L., ed., EPJ Web of Conf., Vol. 61, The Innermost Regions of Relativistic Jets and Their Magnetic Fields. p. 01005
Floyd D. J. E., Dunlop J. S., Kukula M. J., Brown M. J. I., McLure R. J., Baum S. A., O'Dea C. P., 2013, MNRAS, 429, 2
Fukumura K., Kazanas D., Shrader C., Behar E., Tombesi F., Contopoulos I., 2018, ApJ, 864, L27
Giustini M., Proga D., 2019, A&A, 630, A94
Hardcastle M. J. et al., 2023, A&A, 678, A151
Harris C. R. et al., 2020, Nature, 585, 357
Harris K. et al., 2016, MNRAS, 457, 4179
Hewett P. C., Foltz C. B., 2003, AJ, 125, 1784
Higginbottom N., Proga D., Knigge C., Long K. S., Matthews J. H., Sim S. A., 2014, ApJ, 789, 19
Kaspi S., Smith P. S., Netzer H., Maoz D., Jannuzi B. T., Giveon U., 2000, ApJ, 533, 631
Kellermann K. I., Sramek R., Schmidt M., Shaffer D. B., Green R., 1989, AJ, 98, 1195
Klindt L., Alexander D. M., Rosario D. J., Lusso E., Fotopoulou S., 2019, MNRAS, 488, 3109
Konigl A., Kartje J. F., 1994, ApJ, 434, 446
Kratzer R. M., Richards G. T., 2015, AJ, 149, 61
Kukula M. J., Dunlop J. S., Hughes D. H., Rawlings S., 1998, MNRAS, 297, 366
Lacy M., Laurent-Muehleisen S. A., Ridgway S. E., Becker R. H., White R. L., 2001, ApJ, 551, L17
Laha S., Reynolds C. S., Reeves J., Kriss G., Guainazzi M., Smith R., Veilleux S., Proga D., 2021, Nat. Astron., 5, 13
Laor A., 2000, ApJ, 543, L111
Laor A., Behar E., 2008, MNRAS, 390, 847
Leighly K. M., Moore J. R., 2004, ApJ, 611, 107
Lucy L. B., Solomon P. M., 1970, ApJ, 159, 879
Lyke B. W. et al., 2020, ApJS, 250, 8
Macfarlane C. et al., 2021, MNRAS, 506, 5888
Mathews W. G., Ferland G. J., 1987, ApJ, 323, 456
Matthews J. H. et al., 2023, MNRAS, 526, 3967
McLure R., Dunlop J., 2001, in Márquez I., Masegosa J., Del Olmo A., Lara L., García E., Molina J., eds, QSO Hosts and Their Environments. Kluwer Academic, Dordrecht, p. 27
McLure R. J., Jarvis M. J., 2002, MNRAS, 337, 109
McLure R. J., Jarvis M. J., 2004, MNRAS, 353, L45
Mehdipour M., Costantini E., 2019, A&A, 625, A25
Metcalf R. B., Magliocchetti M., 2006, MNRAS, 365, 101
Miller L., Peacock J. A., Mead A. R. G., 1990, MNRAS, 244, 207
Mizumoto M., Done C., Tomaru R., Edwards I., 2019, MNRAS, 489, 1152
Moderski R., Sikora M., Lasota J. P., 1998, MNRAS, 301, 142
Morabito L. K. et al., 2019, A&A, 622, A15
Murray N., Chiang J., Grossman S. A., Voit G. M., 1995, ApJ, 451, 498
Neilsen J., Lee J. C., 2009, Nature, 458, 481
Nemmen R. S., Tchekhovskoy A., 2015, MNRAS, 449, 316
Nims J., Quataert E., Faucher-Giguère C.-A., 2015, MNRAS, 447, 3612
Osterbrock D. E., 1993, ApJ, 404, 551
Owocki S. P., Cranmer S. R., Blondin J. M., 1994, ApJ, 424, 887
Padovani P., 2016, A&AR, 24, 13
Padovani P. et al., 2017, A&AR, 25, 2
Panessa F., Baldi R. D., Laor A., Padovani P., Behar E., McHardy I., 2019, Nat. Astron., 3, 387
Pedregosa F. et al., 2011, J. Mach. Learn. Res., 12, 2825
Peterson B. M., 1997, An Introduction to Active Galactic Nuclei. Cambridge Univ. Press, Cambridge
Petley J. W. et al., 2022, MNRAS, 515, 5159
Petley J. W. et al., 2024, MNRAS, 529, 1995
Proga D., 2000, ApJ, 538, 684
Proga D., Stone J. M., Kallman T. R., 2000, ApJ, 543, 686
Punsly B., Zhang S., 2011, MNRAS, 412, L123
Rankine A. L., Hewett P. C., Banerji M., Richards G. T., 2020, MNRAS, 492, 4553
Rankine A. L., Matthews J. H., Hewett P. C., Banerji M., Morabito L. K., Richards G. T., 2021, MNRAS, 502, 4154
Rees M. J., Begelman M. C., Blandford R. D., Phinney E. S., 1982, Nature, 295, 17
Ricarte A., Narayan R., Curd B., 2023, ApJ, 954, L22
Richards G. T. et al., 2006, ApJS, 166, 470
Richards G. T. et al., 2011, AJ, 141, 167

Richards G. T., McCaffrey T. V., Kimball A., Rankine A. L., Matthews J. H., Hewett P. C., Rivera A. B., 2021, AJ, 162, 270
Rosario D. J., Fawcett V. A., Klindt L., Alexander D. M., Morabito L. K., Fotopoulou S., Lusso E., Calistro Rivera G., 2020, MNRAS, 494, 3061
Sabater J. et al., 2019, A&A, 622, A17
Sandage A., 1965, ApJ, 141, 1560
Sbarrato T., Ghisellini G., Giovannini G., Giroletti M., 2021, A&A, 655, A95
Schmidt M., 1969, ARA&A, 7, 527
Shapiro S. L., 2005, ApJ, 620, 59
Shen Y. et al., 2011, ApJS, 194, 45
Shimwell T. W. et al., 2019, A&A, 622, A1
Shimwell T. W. et al., 2022, A&A, 659, A1
Stepney M., Banerji M., Hewett P. C., Temple M. J., Rankine A. L., Matthews J. H., Richards G. T., 2023, MNRAS, 524, 5497
Stocke J. T., Morris S. L., Weymann R. J., Foltz C. B., 1992, ApJ, 396, 487
Sulentic J. W. et al., 2017, A&A, 608, A122
Talbot R. Y., Bourne M. A., Sijacki D., 2021, MNRAS, 504, 3619
Tchekhovskoy A., 2015, in Contopoulos I., Gabuzda D., Kylafis N., eds, Astrophysics and Space Science Library, Vol. 414, The Formation and Disruption of Black Hole Jets. Springer International Publishing, Switzerland, p. 45
Temple M. J., Hewett P. C., Banerji M., 2021, MNRAS, 508, 737
Temple M. J. et al., 2023, MNRAS, 523, 646
Timlin J. D., III, Brandt W. N., Laor A., 2021, MNRAS, 504, 5556
van Haarlem M. P. et al., 2013, A&A, 556, A2
Vestergaard M., Osmer P. S., 2009, ApJ, 699, 800
Virtanen P. et al., 2020, Nat. Methods, 17, 261
Volonteri M., Madau P., Quataert E., Rees M. J., 2005, ApJ, 620, 69
Wandel A., Peterson B. M., Malkan M. A., 1999, ApJ, 526, 579
Wang H., Wang T., Zhou H., Liu B., Wang J., Yuan W., Dong X., 2011, ApJ, 738, 85
Wardle M., Koenigl A., 1993, ApJ, 410, 218
Waskom M. L., 2021, J. Open Source Softw., 6, 3021
White R. L., Helfand D. J., Becker R. H., Gregg M. D., Postman M., Lauer T. R., Oegerle W., 2003, AJ, 126, 706
Whittam I. H. et al., 2022, MNRAS, 516, 245
Woods D. T., Klein R. I., Castor J. I., McKee C. F., Bell J. B., 1996, ApJ, 461, 767
Wu X.-B. et al., 2015, Nature, 518, 512
Xie W., Lei W.-H., Zou Y.-C., Wang D.-X., Wu Q., Wang J.-Z., 2012, Res. Astron. Astrophys., 12, 817
Yue B. H. et al., 2024, MNRAS, 529, 3939
Yue B. H. et al., 2025, MNRAS, 537, 858
Zakamska N. L., Greene J. E., 2014, MNRAS, 442, 784
Zhang L., Fan J., Zhu J., 2021, PASJ, 73, 313

APPENDIX A: IMPACT OF RADIO-LOUD CLASSIFICATION SCHEME

This appendix shows versions of the plots in the body of the paper using the other two radio-loud classification methods: the traditional radio loudness ratio cut ($\log(R) > 2.5$) and the use of a radio luminosity threshold ($L_{144} > 10^{26}$W Hz^{-1}).

We perform the same NearestNeighbours matching procedure in L_{3000} and FWHM$_{\rm Mg\ II}$ space as we did for the GMM-defined RL and RQ populations. The classical $\log(R)$ cut has a resulting 2D KS test p-value of 0.999 in the matched parameter space, and the L_{144} cut has a p-value of 0.998. Both of these are thus statistically indistinguishable, and the distributions before and after matching are shown in Fig. A1 for the $\log(R) > 2.5$ criteria, and in Fig. A2 for $L_{144} > 10^{26}$W Hz^{-1}.

We show the distributions of C IV blueshift and EW$_{\rm C\ IV}$ for the matched populations as defined by the $\log(R)$ and the L_{144} cuts in Fig. A3. It is clear that the difference in blueshift between the RL and RQ quasars is insensitive to the choice of radio loudness

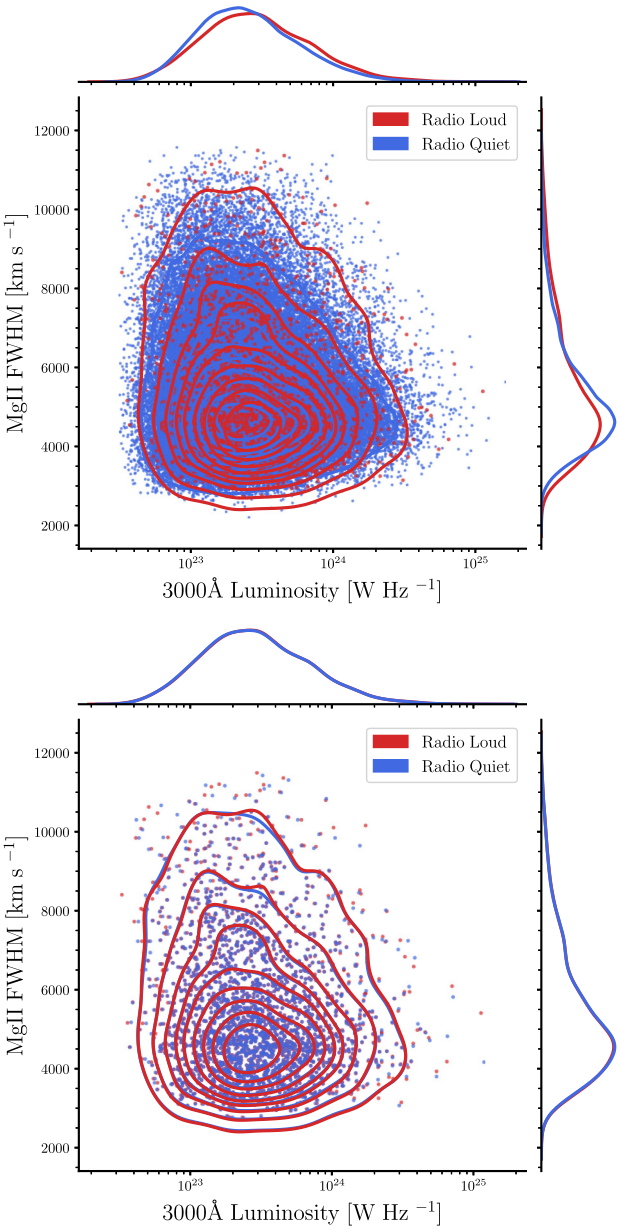

Figure A1. Distributions of radio-loud (red points/contours) and radio-quiet (blue points/contours) quasars in L_{3000} and FWHM$_{\rm Mg\ II}$ space, for the entire sample (top) and then after NearestNeighbour matching in this space (bottom). The RL and RQ populations are as defined by the radio loudness ratio cut. As in Fig. 3, the matching procedure has resulting in indistinguishable distributions in both properties for RL and RQ sources.

classification method: in all cases, RL quasars display weaker blueshifts than their RQ counterparts (and, presumably, weaker disc winds), even when accounting for differences in black hole mass and Eddington fraction. The distinction in EW$_{\rm C\ IV}$ is less clear, however, with the resulting difference being greater for the luminosity cut defined samples, but less for the traditional radio loudness method. However, the resulting KS-test p-values are 2.30×10^{-20} and 4.7×10^{-4} respectively, and therefore the null hypothesis of the RL and RQ populations being drawn from the same distribution can be rejected. That means that, statistically,

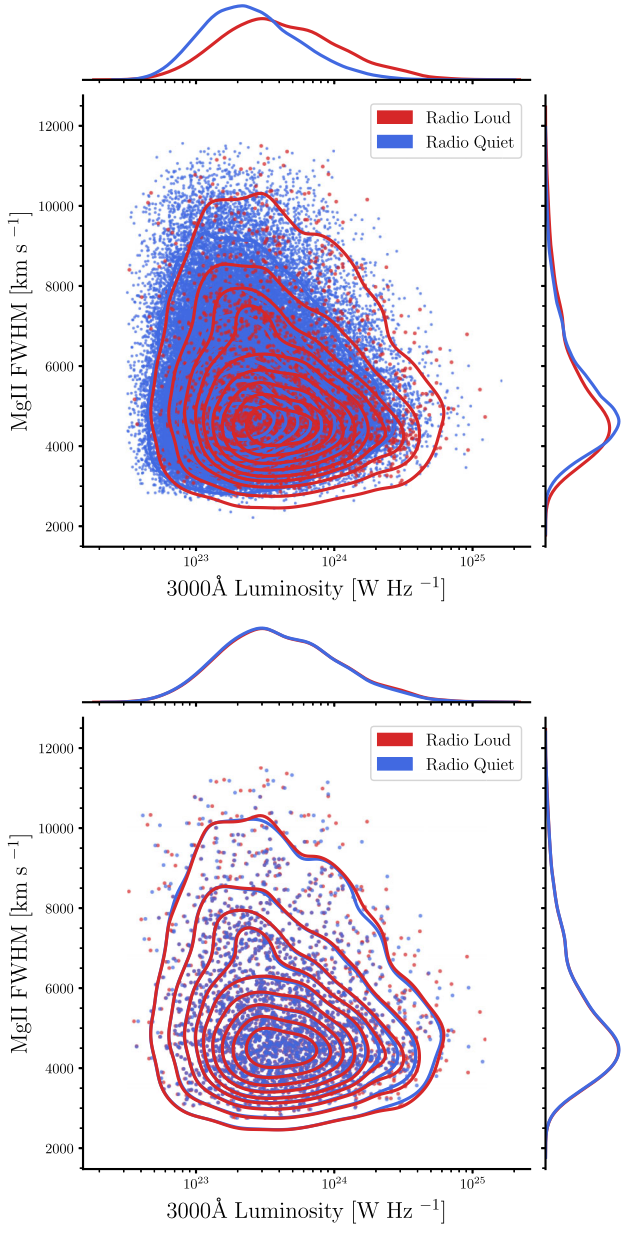

Figure A2. Distributions of radio-loud (red points/contours) and radio-quiet (blue points/contours) quasars in L_{3000} and FWHM$_{\rm Mg\ II}$ space, for the entire sample (top) and then after NearestNeighbour matching in this space (bottom). The RL and RQ populations are as defined by the radio luminosity cut ($L_{144} > 10^{26}$W Hz^{-1}). As in Fig. 3, the matching procedure has resulting in indistinguishable distributions in both properties for RL and RQ sources.

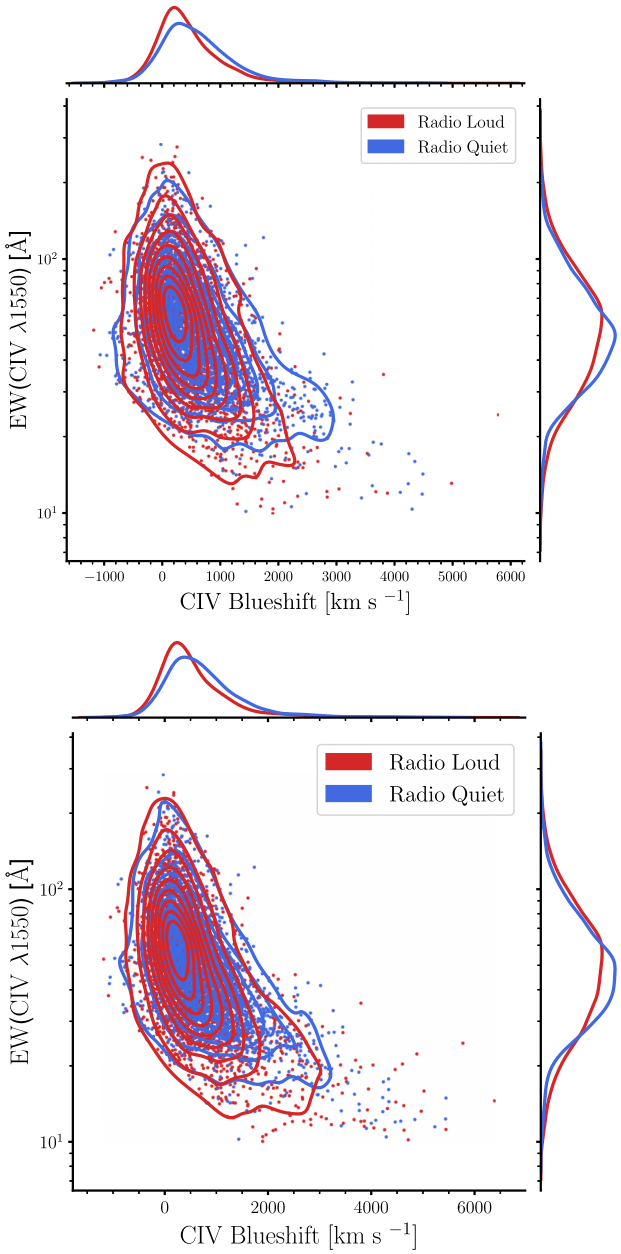

Figure A3. The C IV blueshift and EW$_{\rm C\ IV}$ distributions for radio-loud (red points/contours) and radio-quiet (blue points/contours) quasars, for the radio loudness ratio cut ($\log_{10}(R) > 2.5$, top) and then radio luminosity cut ($L_{144} > 10^{26}$W Hz^{-1}, right). The distributions show the populations after matching in L_{3000} and FWHM$_{\rm Mg\ II}$. The trends found in Fig. 4 are consistent across the classification methods.

despite the RL and RQ EW$_{\rm C\ IV}$ distributions appearing similar for all three classification methods, they are formally different.

This has implications for the Baldwin effect investigation, which is reproduced for the two alternate classification methods in Figs A4 and A5. Again, the conclusion that there is a slightly different Baldwin effect in RL and RQ quasars is invariant under our different RL classification methods.

We recreate the investigation of emission line properties in black hole mass and Eddington fraction space from Fig. 7 in Fig. A6 for the radio loudness cut and radio luminosity cut defined populations, respectively. The main results are the same across all three figures. In all cases, there is an anticorrelation between the strength of C IV blueshift and the EW of the C IV and He II lines, and RQ sources with very high black hole masses ($M_{\rm BH} > 10^9 M_\odot$) and Eddington fractions $\lambda_{\rm Edd} > 0.1$ show very strong C IV blueshifts, but the equivalent RL sources do not. However, in the L_{144} defined method, the differences between trends in the RL and RQ sources are slightly less pronounced. It could be inferred that the presence of sources displaying 'RQ-like' properties in the RL sample (i.e. strong C IV blueshifts at high

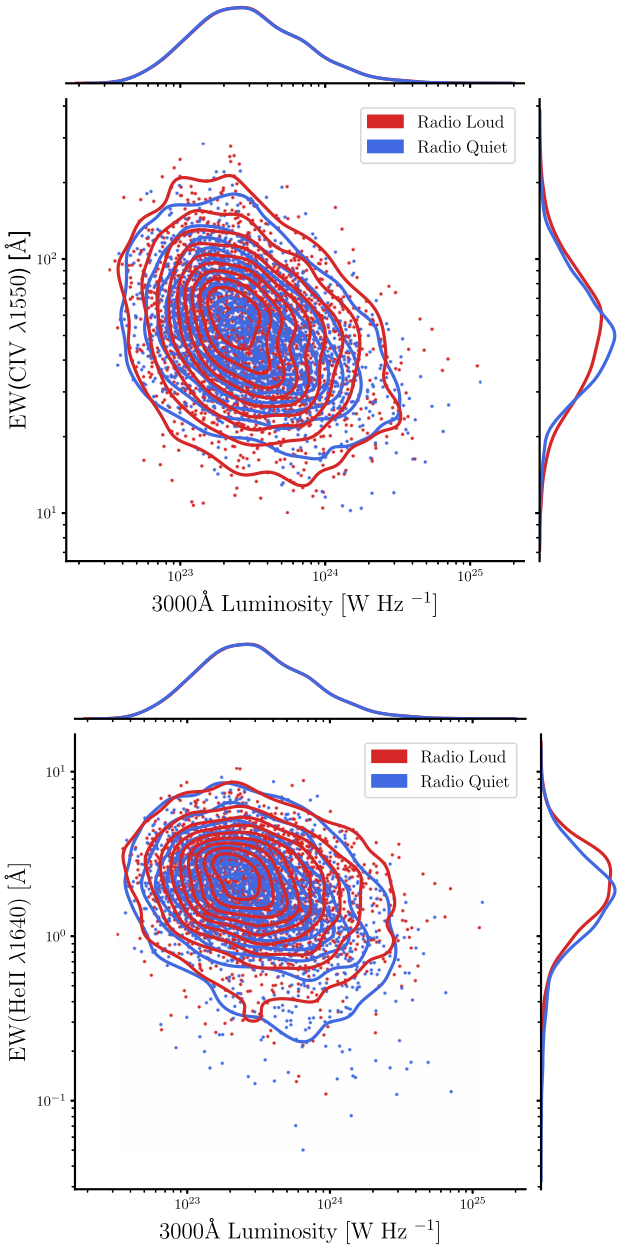

Figure A4. Ultraviolet emission line EWs for radio-loud (red points/contours) and radio-quiet (blue points/contours) quasars matched in L_{3000} and $\mathrm{FWHM_{Mg\,II}}$, against L_{3000}. This is effectively a test of the Baldwin effect. The plots on the top row show distribution of $\mathrm{EW_{C\,IV}}$ against L_{3000}, and the bottom row shows the same, but for He II. The populations in this plot are defined by the use of a $\log_{10}(R)$ cut. The trends found in Fig. 5 are also seen in this plot, and are therefore not dependant on the choice of classification method.

M_{BH} and λ_{Edd}) may be a result of contamination from non-jetted sources that we have hypothesized maybe classified as RL as a result of using the method throughout the discussion of the cuts.

Finally, in Figs A7 and A8, we reproduce Fig. 9. The results of the $\log_{10}(R)$ cut are generally consistent with the results produced by the GMM-defined populations, except for the highest black hole masses ($M_{\mathrm{BH}} > 10^{9.36}\mathrm{M}_{\odot}$) and highest Eddington fractions ($\lambda_{\mathrm{Edd}} > 0.15$), where there is an even greater decrease in RL fraction whilst the other property is high. In the $L_{144} > 10^{26}\mathrm{W\ Hz^{-1}}$ case, for all Eddington fraction and black hole mass bins, the fraction of radio-loud sources increases with the two properties. In the latter case, this is a result of the general increase of L_{144} with L_{3000}, meaning that as either black hole mass or Eddington fraction increases, more sources meet the radio luminosity threshold (see equations 1 and 2). In the former case, it is the opposite: for the highest black hole mass and Eddington fraction objects, a source must have significantly higher radio emission to compete with the prodigious optical luminosity, causing a decrease in RL fraction.

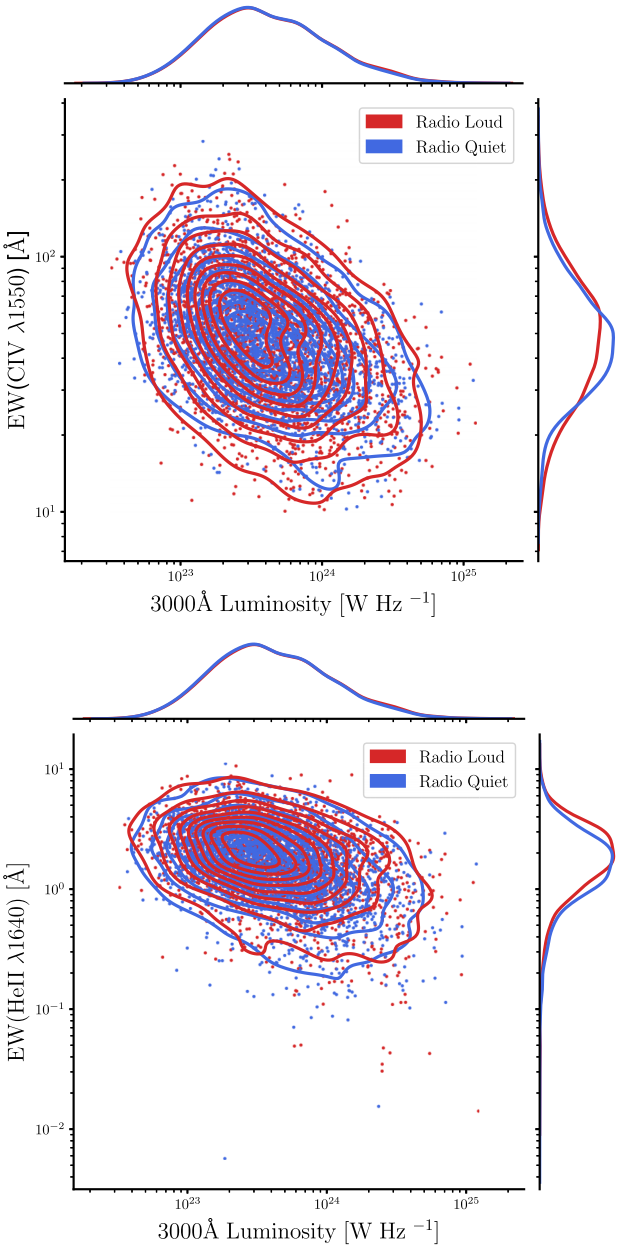

Figure A5. Ultraviolet emission line EWs for radio-loud (red points/contours) and radio-quiet (blue points/contours) quasars matched in L_{3000} and $\mathrm{FWHM_{Mg\,II}}$, against L_{3000}. This is effectively a test of the Baldwin effect. The plots on the top row show distribution of $\mathrm{EW_{C\,IV}}$ against L_{3000}, and the bottom row shows the same, but for He II. The populations in this plot are defined by the use of a L_{144} cut. The trends found in Fig. 5 are also seen in this plot, and are therefore not dependant on the choice of classification method.

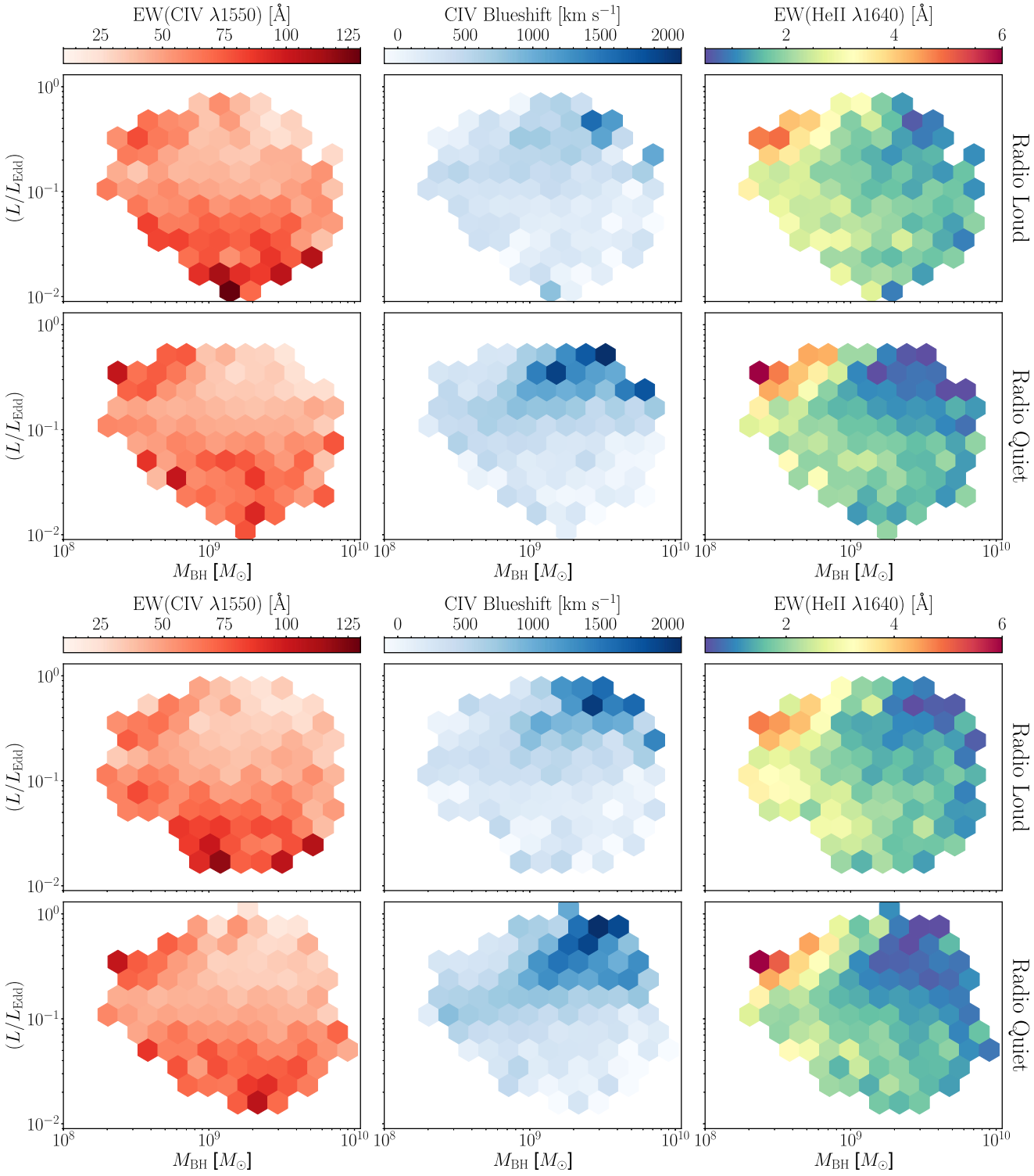

Figure A6. Ultraviolet emission line properties in bins of black hole mass and Eddington fraction space for the radio loudness (top) and radio luminosity (bottom) defined samples, that have been matched in the equivalent of black hole mass and Eddington fraction. As in Fig. 7, the top row of each panel shows the average value of each property for radio loud (top row) and radio quiet (bottom row) sources. The colour scales show, from left to right, the average (median) value of $EW_{C\ IV}$, C IV blueshift, and $EW_{C\ IV}$. The trends seen in Fig. 7 are consistent across all three methods of radio loud classification.

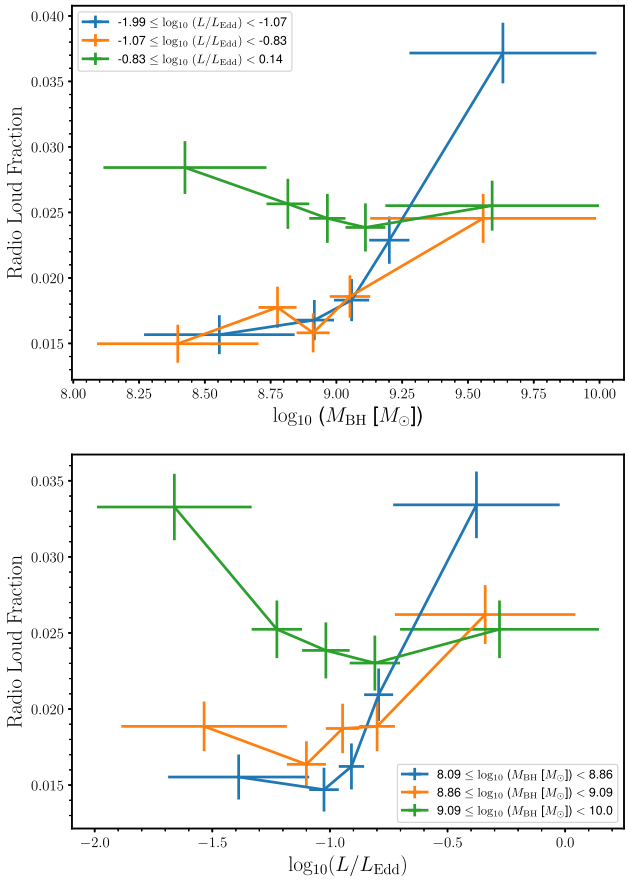

Figure A7. The distribution of radio-loud fraction with increasing black hole mass (top panel) and Eddington fraction (bottom panel). As in Fig. 9, the coloured lines correspond to bins of Eddington fraction (top) and black hole mass (bottom), to show the cumulative effect of the two properties on the radio-loud fraction. This version of the plot shows the results for RL and RQ populations defined by a classical radio loudness ratio criteria.

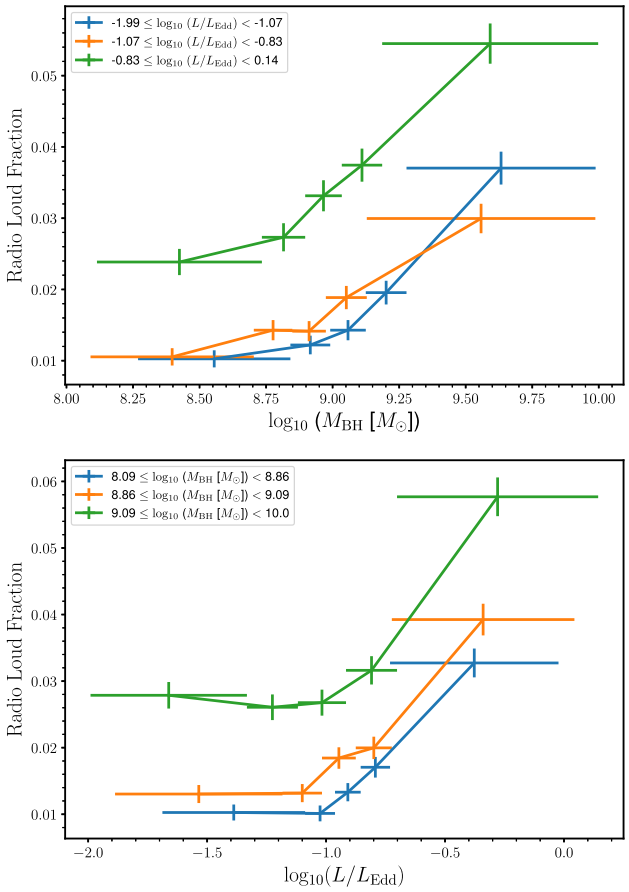

Figure A8. The distribution of radio-loud fraction as a function of black hole mass and Eddington fraction, as in Figs 9 and A7. This plot shows the results of the use of the radio luminosity cut.

This paper has been typeset from a TEX/LATEX file prepared by the author.